Inorganic Chemistry

Article

pubs.acs.org/IC

Cavitands Incorporating a Lewis Acid Dinickel Chelate Function as Receptors for Halide Anions

Alexander Jeremies,[†] Ulrike Lehmann,[†] Sina Gruschinski,[†] Frederik Schleife,[†] Michel Meyer,*[,‡] Vitaly Matulis,[§] Oleg A. Ivashkevich,[∥] Marcel Handke,[†] Karolin Stein,[†] and Berthold Kersting*[,†]

[†]Institut für Anorganische Chemie, Universität Leipzig, Johannisallee 29, 04103 Leipzig, Germany

[‡]Institut de Chimie Moléculaire de l'Université de Bourgogne (ICMUB), UMR CNRS 6302, 9, avenue Alain Savary, BP 47870, 21078 Dijon Cedex, France

[§]Research Institute for Physical Chemical Problems, Belarusian State University, Leningradskaya 14, 220030 Minsk, Belarus

[∥]Belarusian State University, 4 Nezavisimisti avenue, 220050 Minsk, Belarus

Supporting Information

ABSTRACT: The halide binding properties of the cavitand $[Ni_2(L^{Me2H4})]^{2+}$ (**4**) are reported. Cavitand **4** exhibits a chelating $N_3Ni(\mu\text{-}S)_2NiN_3$ moiety with two square-pyramidal $Ni^{II}N_3S_2$ units situated in an anion binding pocket of ~4 Å diameter formed by the organic backbone of the $(L^{Me2H4})^{2-}$ macrocycle. The receptor reacts with fluoride, chloride (in MeCN/MeOH), and bromide (in MeCN) ions to afford an isostructural series of halogenido-bridged complexes $[Ni_2(L^{Me2H4})(\mu\text{-Hal})]^+$ (Hal = F^- (**5**), Cl^- (**6**), and Br^- (**7**)) featuring a $N_3Ni(\mu\text{-}S)_2(\mu\text{-Hal})NiN_3$ core structure. No reaction occurs with iodide or other polyatomic anions (ClO_4^-, NO_3^-, HCO_3^-, $H_2PO_4^-$, HSO_4^-, SO_4^{2-}). The binding events are accompanied by discrete UV−vis spectral changes, due to a switch of the coordination geometry from square-pyramidal (N_3S_2 donor set in **4**) to octahedral in the halogenido-bridged complexes (N_3S_2Hal donor environment in **5**−**7**). In MeCN/MeOH (1/1 v/v) the log K_{11} values for the 1:1 complexes are 7.77(9) (F^-), 4.06(7) (Cl^-), and 2.0(1) (Br^-). X-ray crystallographic analyses for **4**$(ClO_4)_2$, **4**$(I)_2$, **5**(F), **6**(ClO_4), and **7**(Br) and computational studies reveal a significant increase of the intramolecular distance between two propylene groups at the cavity entrance upon going from F^- to I^- (for the DFT computed structure). In case of the receptor **4** and fluorido-bridged complex **5**, the corresponding distances are nearly identical. This indicates a high degree of preorganization of the $[Ni_2(L^{Me2H4})]^{2+}$ receptor and a size fit mismatch of the receptor binding cavity for anions larger than F^-.

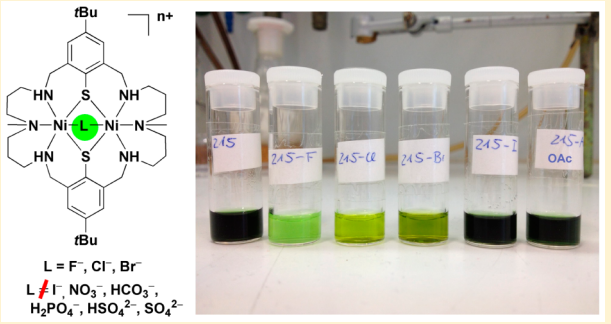

INTRODUCTION

Since the seminal work of Simmons and Park,[1] the host−guest chemistry of macrocyclic anion receptors has been extensively investigated, and more sophisticated examples with better size-complementarity and higher degrees of preorganization[2] have been reported.[3,4] A particularly large amount of work has been devoted to the design of artificial halide receptors with the goal to design molecular-based sensors, receptors, and transporters.[5,6] Designing a selective halide host is very challenging, given that the halide ions behave like spherical charges adopting various coordination geometries without specific binding sites.[7] As with cation hosts selectivity is generally enhanced for cyclic or polycyclic structures, although acyclic structures exhibit interesting halide-binding properties and selectivity as well.[8]

One very successful approach to bind halide anions is chelation by Lewis acids,[9] and several examples of multidentate Lewis-acids incorporating d-block and p-block metals have now been reported.[10] Of these, the cascade complexes with closed-shell structures have received much attention.[11−13] The analogous chemistry of metallocavitands featuring an open binding site has been investigated far less frequently.[14−16]

Recently, we described the binuclear complex $[Ni_2(L^{H6})]^{2+}$ (**1**) supported by the macrocycle H_2L^{H6} (Figure 1).[17] Although being coordinatively unsaturated, the $[Ni_2(L^{H6})]^{2+}$ dication has no affinity for halide ions, in striking contrast to nickel complexes supported by smaller N_6S_2 macrocycles with lateral diethylene triamine linkers[18,19] and other chelating ligands.[20−22] We reasoned that partial N-alkylation would decrease the ligand-field strength of the macrocycle to access coordination numbers higher than 5, thereby generating an active receptor. In this Paper we show that the corresponding $[Ni_2(L^{Me2H4})]^{2+}$ complex (**4**)[23] strongly binds the small spherical fluoride and chloride ions in acetonitrile/methanol solution, has little affinity for the larger bromide ion, and has essentially no affinity for iodide or polyatomic ions of trigonal-planar or tetrahedral geometry. This behavior is discussed in

Received: January 19, 2015
Published: April 6, 2015

DOI: 10.1021/acs.inorgchem.5b00123
Inorg. Chem. 2015, 54, 3937−3950

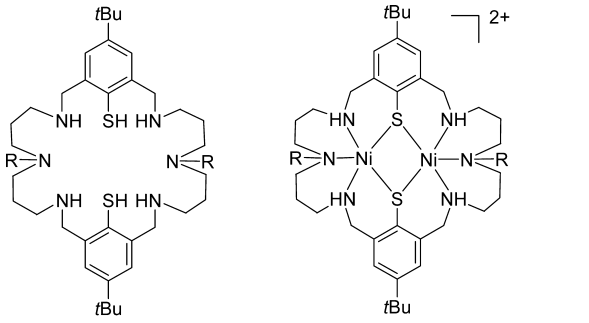

Figure 1. Structure of supporting ligands H_2L^{H6} and H_2L^{Me2H4}, complex **1**, and receptor **4**.[23]

the light of the confined binding cavity and preorganization of **4**.

RESULTS AND DISCUSSION

The targeted supporting ligand H_2L^{Me2H4} was prepared in two steps starting from known tetraaldehyde **2** (Scheme 1). A [2 + 1] condensation reaction between **2** and N^1-(3-aminopropyl)-N^1-methylpropane-1,3-diamine, followed by $NaBH_4$ reduction provided bicyclic macrocycle **3** whose thioether linkage was subsequently cleaved by Na/NH_3. The free macrocycle was isolated as an air-stable hexahydrobromide salt in 62% overall yield (based on **2**). ^1H NMR and ^{13}C NMR spectroscopies, mass spectrometry, and elemental analysis are consistent with the proposed formulation.

Scheme 1. Synthesis of Ligand H_2L^{Me2H4}·6HBr

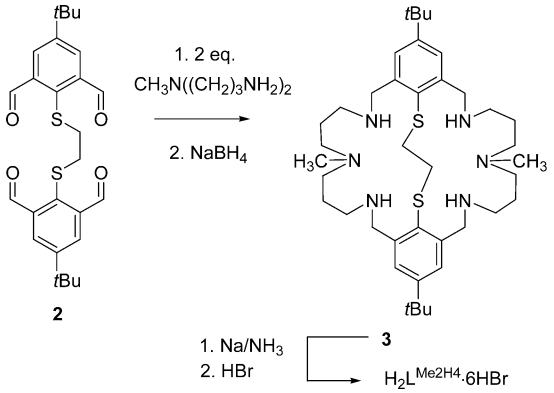

The synthesized complexes and their labels are collected in Scheme 2. Reaction of H_2L^{Me2H4}·6HBr with $NiBr_2·6H_2O$ and NEt_3 in MeOH gave a dark green solution, from which the receptor $[Ni_2(L^{Me2H4})]^{2+}$ (**4**) could be reproducibly isolated as a dark green perchlorate salt in 70% yield. Although isostructural with the parent complex **1**,[17] the host–guest properties of **4** were found to be strikingly different. In contrast to inactive **1**,[24] the dark green receptor **4** reacts readily with fluoride or chloride to form the pale green 1:1 complexes $[Ni_2(L^{Me2H4})(\mu\text{-Hal})]^+$ (Hal = F^- (**5**), Cl^- (**6**)).

The receptor **4** has only little affinity for anions larger than Cl^-. The bromido complex **7** is only accessible in the presence of a large excess of Br^-. An iodido-bridged complex $[Ni_2(L^{Me2H4})(\mu\text{-I})]^+$ (**8**) is inaccessible. Treatment of **4** with I^- produces only the iodide salt $[Ni_2(L^{Me2H4})](I)_2$ (**4**$(I)_2$). Likewise, **4** does not react with polyatomic anions such as OAc^-, HCO_3^-, NO_3^-, SO_4^{2-}, or $H_2PO_4^-$. The higher reactivity of **4** is attributed to the weaker ligand-field strength of the partially N-methylated macrocycle H_2L^{Me2H4}. The structural assignments of receptor **4** and its host–guest complexes **5**–**7** were ascertained through several analytical methods, including IR and UV–vis spectrophotometries, electrospray ionization mass spectrometry (ESI-MS), X-ray diffraction studies (**4**$(ClO_4)_2·4$EtOH, **4**$(I)_2·3t$-BuOH·MeOH, **5**$(F)·5$EtOH·$2H_2O$, **6**$(ClO_4)·2$EtOH·0.5MeOH, and **7**$(Br)·2$MeCN), and density functional theory (DFT) calculations.

Spectroscopic Properties and Anion Binding. The halide binding ability of the dinuclear nickel(II) core embedded inside the molecular pocket of **4** was successfully probed by Fourier transform far-infrared (FT-FIR) spectroscopy (70–700 cm^{-1}). Figure 2 displays an enlargement of the most informative region located between 150 and 350 cm^{-1} (the full-range spectra are available as Supporting Information), where Ni–Hal stretching vibrations are expected to arise. Both spectra corresponding to **4**$(ClO_4)_2$ and **4**$(I)_2$ are strikingly similar in the entire fingerprint area (excepted for the characteristic $\nu(ClO_4)$ band at 621 cm^{-1} which is obviously absent in the spectrum of **4**$(I)_2$), as might be expected if both counteranions are not encapsulated and thus do not interact with the metal centers. The bands at 250 and 235 cm^{-1} in $[Ni_2(L^{Me2H4})](ClO_4)_2$ and $[Ni_2(L^{Me2H4})](I)_2$ are tentatively assigned to the symmetric and antisymmetric Ni–S–Ni stretches. In contrast, this doublet of broad peaks has vanished in the spectra of the F^-, Cl^-, and Br^- complexes. The occurrence of new manifolds peaking at slightly lower energies (~225 and 215 cm^{-1}) in the spectra of complexes **5**–**7** clearly reveals a common behavior when receptor **4** is reacted with any of the three latter anions. The bands centered at 225 and 215 cm^{-1} in the halogenido-brigded $[Ni_2(L^{Me2H4})(\mu\text{-Hal})]^+$ complexes are presumably associated with the symmetric and antisymmetric Ni–S–Ni stretches. Relative to those in **4** these are shifted to lower frequencies. This red-shift is in accordance with the significant lengthening (weakening) of the Ni–S bonds upon halide binding (Supporting Information, Table S1). The thereby evidenced uptake and size discrimination ability of the molecular cavity for the smaller F^-, Cl^-, and Br^- anions with respect to the larger I^- is also fully compatible with the proposed μ-bridging interaction between the guest and the nickel core.

Anion binding by receptor **4** is, moreover, expected to cause distinct spectral changes in the UV–vis–NIR range due to a change of the coordination geometry from square-pyramidal (N_3S_2 donor set in **4**) to octahedral in the halogenido-bridged complexes (N_3S_2Hal donor environment in **5**–**7**). Therefore, all complexes were studied by electronic absorption spectroscopy. Selected electronic absorption data are listed in Table 1 along with spectral assignments. Figure 3 shows the electronic absorption spectra of the compounds in the 500–1400 nm range at a concentration of ~1×10^{-3} M.

As can be seen, solutions of the free receptor $[Ni_2(L^{Me2H4})](ClO_4)_2$ (**4**$(ClO_4)_2$) in MeCN/MeOH (1/1 v/v) are dark green in contrast to the pale green solutions of the halogenido-bridged complexes **5**(ClO_4) and **6**(ClO_4). The four electronic absorption bands at 530, 635, 786, and 1012 nm are typical for square-pyramidal $Ni^{II}N_3S_2$ chromophores[24,25] and can be assigned to the spin-allowed $^3B_1 \rightarrow {}^3E$, $^3B_1 \rightarrow {}^3B_2$, $^3B_1 \rightarrow {}^3A_2$, and $^3B_1 \rightarrow {}^3E$ transitions (in pure C_{4v} symmetry). The diffuse reflectance spectrum of microcrystalline **4**$(ClO_4)_2$ (see

DOI: 10.1021/acs.inorgchem.5b00123
Inorg. Chem. 2015, 54, 3937–3950

Scheme 2. Synthesis of Compounds

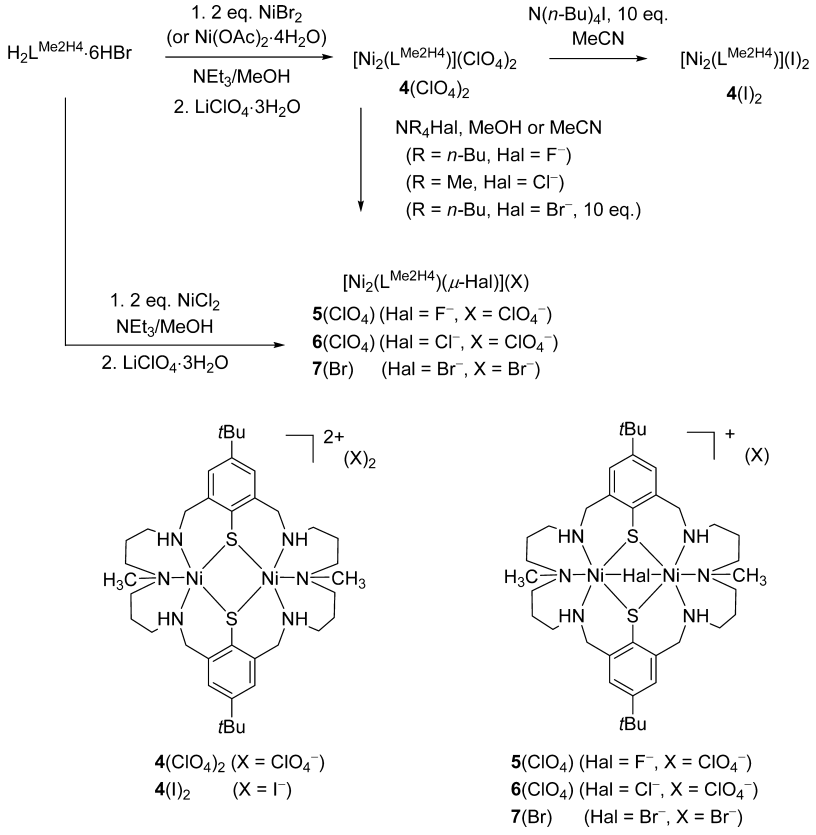

Supporting Information) is not markedly different from that in solution, demonstrating that the solid-state structure (with two square-pyramidal NiN_3S_2 chromophores bridged via the two thiolate atoms) is similar to the solution-state structure.

The spectra of the fluorido- ($\mathbf{5}(ClO_4)$) and chlorido- ($\mathbf{6}(ClO_4)$) bridged complexes in MeCN/MeOH are similar but not identical. Both differ significantly from that of the free receptor $\mathbf{4}(ClO_4)_2$. Two bands attributable to d−d transitions ($\nu_2(^3A_{2g} \rightarrow {}^3T_{1g})$ and $\nu_1(^3A_{2g} \rightarrow {}^3T_{2g})$) of a distorted octahedral $Ni^{II}N_3S_2Hal$ chromophore are detected above 500 nm. The ν_2 transition occurs in the 620−650 nm range, and the ν_1 transition is seen between 1020 and 1065 nm. The third d−d transition $\nu_3(^3A_{1g} \rightarrow {}^3T_{1g}(P))$ expected for an octahedral NiN_3S_2Cl complex at ∼400 nm cannot be detected as it is obscured by more intense $\pi-\pi^*$ transitions within the aromatic rings of the supporting ligand.[26] Each compound reveals also a weak shoulder around 915 nm attributable to a spin-forbidden $^3A_{2g} \rightarrow {}^1E_g$ (D) transition, which gains intensity due to the deviation from pure octahedral symmetry. The diffuse reflectance spectra of $\mathbf{5}(ClO_4)$ and $\mathbf{6}(ClO_4)$ are very similar to those in solution showing that the complex integrity is maintained upon dissolution. Thus, the two complexes **5** and **6** retain their solid-state structures in polar aprotic as well as protic solvents.[27]

In contrast to $\mathbf{5}(ClO_4)$ and $\mathbf{6}(ClO_4)$, the spectral properties of $\mathbf{7}(Br)$ are strongly solvent-dependent. In neat acetonitrile the compound is pale green, and the three absorption bands at 651, 926, and 1065 nm for an octahedral $Ni^{II}N_3S_2Br$ chromophore confirm the presence of the bromido-bridged complex $[Ni_2(L^{Me2H4})(\mu\text{-}Br)](Br)$. The red-shift of the ν_1 transition from 1022 nm for **5** to 1065 nm for **7**[28] also nicely correlates with the lower ligand-field strength of the bromido ligand.

Dissolving the pale green salt $\mathbf{7}(Br)$ in MeCN/MeOH (1/1 v/v) results in an immediate color change to dark green, and the four bands at 534, 635, 784, and 1015 nm clearly show the presence of substantial amounts of the free receptor **4**, which forms upon dissociation of the bromido complex **7** as indicated by eq 1. The spectrum in pure MeOH shows a hyperchromic effect for the main features at 635 and 786 nm indicating that dissociation of **7** is more pronounced and that the presence of methanol in the solvent promotes the liberation of the bromido ligand. The ESI-MS spectrum confirms that $\mathbf{7}(Br)$ dissociates in MeCN/MeOH (1/1 v/v), since two molecular ion peaks, one for the dication **4** (m/z = 392.2) and one for the bromido complex **7** (m/z = 865.2), can be detected. The influence of solvent on the stability of complex **7** can be traced to a competing solvation reaction of the bromide ion by methanol molecules. Such solvent effects are quite common in molecular recognition[29] and play a crucial role in anion recognition.[30,31] For **5** and **6**, binding of the halide ions by the Ni^{2+} ions is much stronger and the equilibria are much less sensitive to the choice of solvent.

$$[Ni_2(L^{Me2H4}_{7})(\mu\text{-}Br)]^+ \rightleftharpoons [Ni_2(L^{Me2H4}_{4})]^{2+} + Br^- \quad (1)$$

As it is shown below, crystals of $\mathbf{4}(I)_2 \cdot 3t\text{-}BuOH \cdot MeOH$ comprise the free receptor **4**, *t*-BuOH and MeOH solvate molecules, and two iodides as counterions. Therefore, the electronic absorptions of $\mathbf{4}(I)_2$ are expected to be very similar to those of the perchlorate salt of receptor **4**.[32] Indeed, the electronic transitions recorded for $\mathbf{4}(I)_2$ in solution as well as in the solid state (diffuse reflectance) match quite well with those determined for $\mathbf{4}(ClO_4)_2$. This match in values clearly demonstrates that **4** does not bind iodide. Further experiments

DOI: 10.1021/acs.inorgchem.5b00123
Inorg. Chem. 2015, 54, 3937−3950

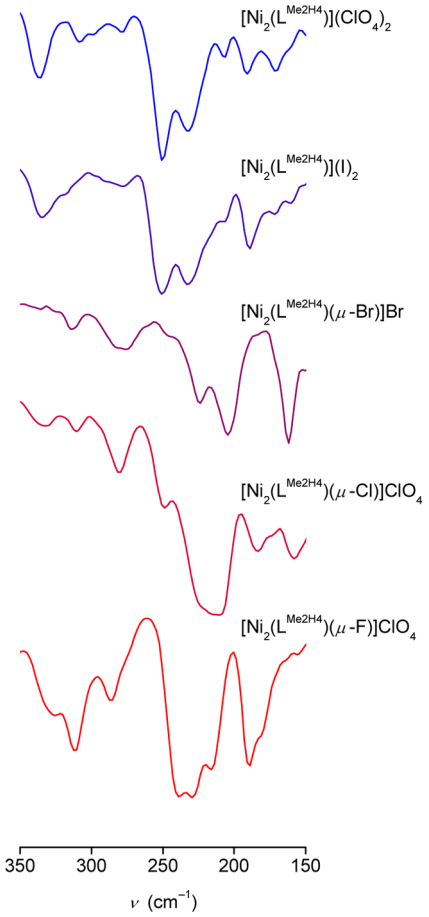

Figure 2. Attenuated total reflectance FT-FIR spectra of $[Ni_2(L^{Me2H4})](ClO_4)_2$ (**4**$(ClO_4)_2$), $[Ni_2(L^{Me2H4})](I)_2$ (**4**$(I)_2$), $[Ni_2(L^{Me2H4})(\mu\text{-F})](ClO_4)$ (**5**(ClO_4)), $[Ni_2(L^{Me2H4})(\mu\text{-Cl})](ClO_4)$ (**6**(ClO_4)), and $[Ni_2(L^{Me2H4})(\mu\text{-Br})](Br)$ (**7**(Br)).

have shown that the spectral properties of receptor **4**$(ClO_4)_2$ do not change in the presence of trigonal-planar or tetrahedral oxo ions such as ClO_4^-, NO_3^-, $H_2PO_4^-$, HSO_4^-, and SO_4^{2-}, suggesting that **4** has no affinity for them.[33]

There are not many examples of compounds in the literature whose properties can be compared to those of **4**.[34] A relevant Ni(II) complex, $[Ni(L)(OH_2)_2]^{2+}$, supported by a 14-membered dithia–diaza macrocycle L, has been described.[34] As in the case of **4**, this complex reacts with F^-, Cl^-, and Br^- to form halogenido-bridged $[\{Ni(L)\}_2(\mu\text{-}X)_2]^{2+}$ structures. Unlike **4**, however, it also forms a complex $[Ni(L)(I)(OH_2)]^+$ with a monodentate iodide ligand. This receptor appears to be less preorganized than **4**.

Determination of Stability Constants. A series of UV–vis–NIR spectrophotometric titrations were performed to quantify the binding strengths and selectivities of receptor **4** for the halide ions F^-, Cl^-, and Br^-; see eq 2.

$$[Ni_2(L^{Me2H4})]^{2+} + Hal^- \rightleftharpoons [Ni_2(L^{Me2H4})(\mu\text{-Hal})]^+ \quad K_{11}$$
$$(Hal = F^-, Cl^-, Br^-) \qquad (2)$$

The titrations were performed in a MeCN/MeOH (1/1 v/v) solvent mixture, because the binding constants in MeCN (for **5** and **6**) were found to be too high to be measured directly by spectrophotometry. Figure 4 shows the spectral changes that occur upon addition of $N(n\text{-}Bu)_4F$ to ca. 1×10^{-2} and 1×10^{-5} M solutions of receptor **4** in the 450–1500 nm and the 190–400 nm regions, respectively. Up to the addition of 1 equiv of fluoride salt, the appearance of the characteristic absorption bands at 622 and 1024 nm, and the disappearance of the absorption features characteristic of **4** at 635 and 786 nm, clearly confirm the immediate formation of the fluorido-bridged complex **5**. However, a close examination of the 890 and 1235 nm regions of Figure 4a clearly evidences the absence of isosbestic points. It can also be seen that the intensities of the 622 and 1024 nm bands start to decrease above a 1:1 molar ratio. This behavior is indicative for the formation of a new, less stable species, which is believed to be a $[Ni_2(L^{Me2H4})(\mu\text{-F})]^+\cdots F^-$ contact ion pair, held together by a $NH\cdots F^-$ hydrogen bonding interaction as shown in Supporting Information, Figure S1. Given that $NH\cdots F^-$ hydrogen bonds are strong[35] and that similar NH···Hal hydrogen bonds are seen in the crystal structures of **4**$(I)_2\cdot 3t$-BuOH·MeOH (Supporting Information, Figure S14), **5**(F)·5EtOH·$2H_2O$ (Supporting Information, Figure S2), and **7**(Br)·2MeCN (Supporting Information, Figure S3), this is a plausible structural hypothesis for the 1:2 adduct.[36] In addition, the formation of $NH\cdots F^-$ hydrogen bonds alters slightly the ligand-field strength of the secondary amine donors, which would explain the observed spectral changes occurring at fluoride excesses higher than one. In the 190–400 nm range (Figure 4b), a similar behavior was detected. The bands at 244 (sh), 268 (sh), and 319 nm for **4** shift or vanish with increasing F^- concentration, and the new bands for **5** develop with maxima at 281 and 314 nm, although without showing any sharp isosbestic point as already stressed for the visible range.

Factor analysis by the Specfit program[37] using the data in the 190–400 nm range[38] confirmed that at least three absorbing species significantly contribute to the observed spectral changes. Subsequent nonlinear least-squares refinements by either Specfit[37] or HypSpec 2014[39] converged for a speciation model involving **4**, the 1:1 fluorido complex **5** with an association constant of log K_{11} = 7.77(9), and the fluoride adduct $[Ni_2(L^{Me2H4})(\mu\text{-F})]^+\cdots F^-$ with a stepwise association constant of log K_{12} = 4.54(1) (Supporting Information, Figures S4 and S5). If the latter species is ignored, the goodness of fit is significantly worsened (the weighted standard deviation of the residuals increases by a factor of 4), especially in the spectral range underneath 210 nm where the absorption spectra of $[Ni_2(L^{Me2H4})(\mu\text{-F})]^+\cdots F^-$ and $[Ni_2(L^{Me2H4})(\mu\text{-F})]^+$ are the more differentiated (Supporting Information, Figure S6). It should be mentioned that the value found for K_{11} reaches almost the commonly admitted limit of 1×10^8 for a reliable direct determination of a binding constant, and so the log K values (and their standard error) should be taken as indicative rather than definitive. On the other hand, very similar K_{11} stability constants were obtained by a competition titration—vide infra). Thus, **4** has a very high affinity for fluoride anions, while the fluorido complex **5** is ~3 orders of magnitude more stable than the postulated $[Ni_2(L^{Me2H4})(\mu\text{-F})]^+\cdots F^-$ adduct. In contrast, $[Ni(H_2O)_6]^{2+}$ binds fluoride only very weakly in a 1:1 ratio in the highly competitive solvent H_2O (log K_{11} = 0.66(5), I = 1 M (H,Na)ClO_4, T = 293.2 K).[40] The K_{12} value for the fluoride adduct **5**$\cdots F^-$ is in a typical range for host–guest complexes held together by NH···F hydrogen bonds.[41] Lehn found a log K value of ~4.2 for F^- binding to cryptands in water through multiple H-bonds. In our case, F^- interacts only through a single $NH\cdots F^-$ bond with $[Ni_2L(F)]^+$, but the solvent system is less dissociating. In solvents of low dielectric strength, $NH\cdots F^-$ bonding can become quite strong. Fabbrizzi

DOI: 10.1021/acs.inorgchem.5b00123
Inorg. Chem. 2015, 54, 3937–3950

Table 1. Electronic Absorption Data for Complexes 4−7 in MeCN/MeOH (1/1 v/v), MeCN, and Diffuse Reflectance Spectroscopic Data in the Solid State[a]

medium	λ_{max}/nm (ε_{max}/M^{-1} cm^{-1}) MeCN/MeOH[b]	λ_{max}/nm (ε_{max}/M^{-1} cm^{-1}) MeCN	λ_{max}/nm solid state[c]	assignment
4$(ClO_4)_2$	530 (296)	531 (301)	∼540 sh	$^3B_1 \rightarrow {}^3E$
	635 (448)	635 (454)	633 (s)	$^3B_1 \rightarrow {}^3B_2$
	786 (111)	786 (110)	791 (w)	$^3B_1 \rightarrow {}^3A_2$
	1012 (38)	1012 (35)	1010 (w)	$^3B_1 \rightarrow {}^3E$
4$(I)_2$	526 (301)	529 (306)	∼540 sh	$^3B_1 \rightarrow {}^3E$
	635 (457)	634 (455)	636 (m)	$^3B_1 \rightarrow {}^3B_2$
	786 (111)	786 (116)	∼785 sh	$^3B_1 \rightarrow {}^3A_2$
	1010 (30)	1013 (38)		$^3B_1 \rightarrow {}^3E$
5(ClO_4)	622 (117) [624 (63)][e]	633 (84)	630 (w)	$^3A_{2g} \rightarrow {}^3T_{1g}$ (ν_2)
	∼ 878 sh (42) [913 (26)][e]	∼ 881 sh (826)	∼885 sh	$^3A_{2g} \rightarrow {}^1E_g$ (D)
	1024 (86) [1024 (50)][e]	1022 (66)	957 (w)[d]	$^3A_{2g} \rightarrow {}^3T_{2g}$ (ν_1)
6(ClO_4)	644 (108) [639 (117)][e]	653 (99)	651 (m)	$^3A_{2g} \rightarrow {}^3T_{1g}$ (ν_2)
	∼913 sh (37) [882 (24)][e]	∼914 sh (36)	910 sh	$^3A_{2g} \rightarrow {}^1E_g$ (D)
	1064 (78) [1037 (44)][e]	1062 (76)	1070 (m)	$^3A_{2g} \rightarrow {}^3T_{2g}$ (ν_1)
7(Br)		651 (78)	674 (w)	$^3A_{2g} \rightarrow {}^3T_{1g}$ (ν_2)
		∼926 sh	∼930 (sh)	$^3A_{2g} \rightarrow {}^1E_g$ (D)
		1065 (74)	960 (w)[d]	$^3A_{2g} \rightarrow {}^3T_{2g}$ (ν_1)
	534 (253) [532 (269)][f]			$^3B_1 \rightarrow {}^3E$
	635 (386) [635 (414)][f]			$^3B_1 \rightarrow {}^3B_2$
	784 (94) [786 (98)][f]			$^3B_1 \rightarrow {}^3A_2$
	1015 (35) [1014 (31)][f]			$^3B_1 \rightarrow {}^3E$

[a]UV−vis spectra recorded at ambient temperature. Concentration = 1×10^{-3} M. [b]MeCN/MeOH (1/1 v/v). [c]Intensity: *s* = strong, *m* = medium, *w* = weak; sh denotes a shoulder. [d]This value is approximate as the band overlaps with a measurement artifact. [e]Values in square brackets correspond to solutions containing supporting electrolyte $[N(n\text{-}Bu_4)ClO_4]$ = 0.1 M. [f]Values in square brackets correspond to pure MeOH.

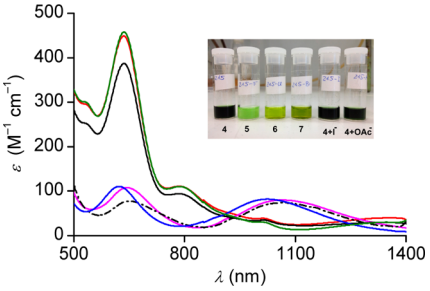

Figure 3. UV−vis−NIR spectra of **4**$(ClO_4)_2$ (red line), **4**$(I)_2$ (green line), fluorido complex **5**(ClO_4) (blue line), and chlorido complex **6**(ClO_4) (magenta line) in MeCN/MeOH (1/1 v/v), and of the bromido complex **7**(Br) in pure MeCN (dashes and dots). The black solid line corresponds actually to the spectrum of **4**$(Br)_2$, which forms upon dissociation of **7**(Br) in MeCN/MeOH (1/1 v/v); see text. Concentration of solutions: 1×10^{-3} M.

has reported a bis-4-nitrophenyl-urea receptor that formed a strong 1:1 complex with just one NH···F^- bond.[42] In MeCN, the log *K* value was found to be 7.38(9).

Addition of a colorless solution of NH_4Cl to a dark green solution of **4** induces a spontaneous color lightening due to the appearance of new absorption bands at 644 and 1064 nm that progressively grow with increasing chloride concentration, while the main absorption features characteristic of **4** centered at 635 ($^3B_1 \rightarrow {}^3B_2$) and 786 nm ($^3B_1 \rightarrow {}^3A_2$) slightly shift to lower energies with a strong hypochromic effect or tend to vanish, respectively (Figure 5). Both isosbestic points developing at 930 and 1302 nm clearly indicate that Cl^- uptake by the dinuclear nickel(II) complex **4** occurs according to a single equilibrium. The exclusive formation of a 1:1 complex (**6**) was ascertained by a Job plot evidencing a clear maximum for an abscissa of 0.5 (1:1 molar ratio). Factor analysis of the entire data set displayed in Figure 5 (21 spectra: 0−2.15 equiv, $450 \leq \lambda \leq 1500$ nm) using the Specfit program[37] further confirmed that only two absorbing species contribute significantly to the observed spectral changes. Subsequent nonlinear least-squares refinements converged for a speciation model involving **4** and its 1:1 chlorido complex **6** with an association constant of log K_{11} = 3.99(4) (Supporting Information, Figures S7 and S8). Accordingly, 99% conversion of **4** into adduct **6** is achieved upon addition of 2 equiv of Cl^-. Refinement of a second data set acquired in the UV range ($190 \leq \lambda \leq 400$ nm) under ca. 200-fold lower concentration levels ($[\mathbf{4}(ClO_4)_2]_0 = 5.02 \times 10^{-5}$ M, $[N(n\text{-}Bu)_4Cl] = 3.4 \times 10^{-4}$ to 3.4×10^{-2} M, 34 spectra: 0−59.7 equiv) and in the presence of 0.01 M $N(n\text{-}Bu)_4ClO_4$ (Supporting Information, Figure S9) converged for log K_{11} = 4.13(3). Considering the much weaker spectrophotometric amplitude in the UV versus visible domain, this value is in excellent agreement with log K_{11} = 3.99(1) found in the millimolar concentration range. In turn, divergence was systematically observed when a second Cl^- binding equilibrium was introduced in the chemical model, as could be expected from the occurrence of isosbestic points at 237, 283, 316, and 333 nm. Noteworthy, binding affinity of **4** for Cl^- in the binary acetonitrile/methanol solvent mixture (1/1 v/v) agrees fairly well with the literature data, as the mean log K_{11} value of 4.06(7) lies in between the stability constants reported for $NiCl^+$ in pure methanol (log K_{11} = 1.3, I = 1 M ($LiClO_4$), T = 298 K)[43] and acetonitrile (log K_{11} = 4.86, I = 0.2 M (NMe_4BF_4), T = 298 K),[44] although the μ-bridging binding

DOI: 10.1021/acs.inorgchem.5b00123
Inorg. Chem. 2015, 54, 3937−3950

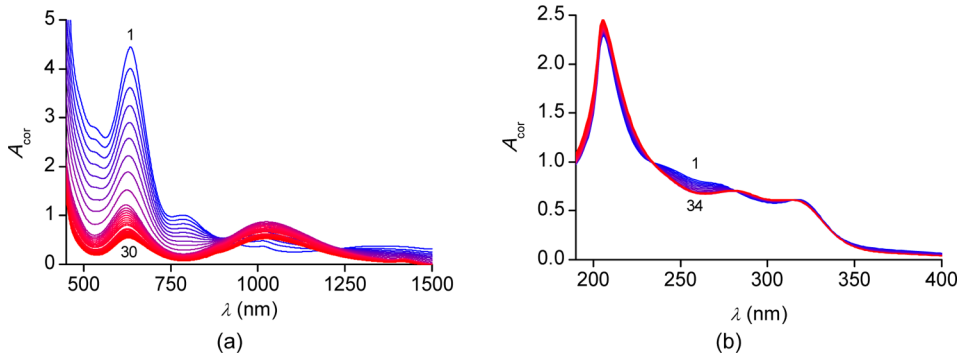

Figure 4. Spectrophotometric titration of the dinickel(II) complex $\mathbf{4}(ClO_4)_2$ as a function of increasing amounts of $N(n\text{-}Bu)_4F$ added in 25 μL increments. Solvent: MeCN/MeOH (1/1 v/v), T = 298(1) K. (a) $[\mathbf{4}(ClO_4)_2]_0 = 9.32 \times 10^{-3}$ M, $[N(n\text{-}Bu)_4F] = 7 \times 10^{-2}$ M (spectra 1−30: 0−3.11 equiv), V_0 = 1.75 mL. (b) $[\mathbf{4}(ClO_4)_2]_0 = 5.02 \times 10^{-5}$ M, $[N(n\text{-}Bu)_4F] = 3.4 \times 10^{-4}$ M (spectra 1−21: 0−2 equiv), $[N(n\text{-}Bu)_4F] = 3.4 \times 10^{-3}$ M (spectra 22−29: 3−10 equiv), $[N(n\text{-}Bu)_4F] = 3.4 \times 10^{-2}$ M (spectra 30−34: 20−60 equiv), supporting electrolyte $[N(n\text{-}Bu)_4ClO_4] = 1 \times 10^{-2}$ M, V_0 = 1.70 mL. All spectra are corrected for dilution effects.

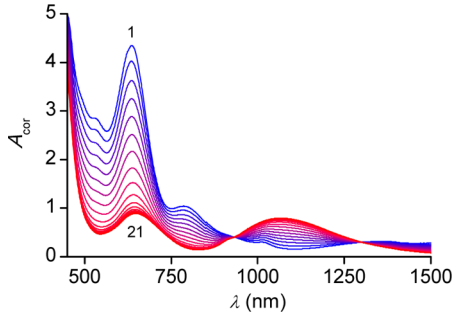

Figure 5. Spectrophotometric titration of the dinickel(II) complex $\mathbf{4}(ClO_4)_2$ as a function of increasing amounts of NH_4Cl added in 25 μL increments. Solvent: MeCN/MeOH (1/1 v/v), T = 298(1) K, $[\mathbf{4}(ClO_4)_2]_0 = 9.32 \times 10^{-3}$ M, $[NH_4Cl] = 7 \times 10^{-2}$ M (spectra 1−21: 0−2.15 equiv), V_0 = 1.75 mL. All spectra are corrected for dilution effects.

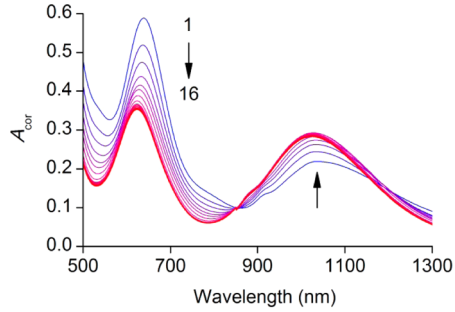

Figure 6. Spectrophotometric titration of the chlorido-bridged complex $\mathbf{6}(ClO_4)$ as a function of increasing amounts of $N(n\text{-}Bu)_4F$ added in 25 μL increments. Solvent: MeCN/MeOH (1/1 v/v), $[\mathbf{6}(ClO_4)] = 4.99 \times 10^{-3}$ M, $[N(n\text{-}Bu)_4F] = 3.39 \times 10^{-2}$ M (spectra 1−16:0−1.50 equiv). Supporting electrolyte $[N(n\text{-}Bu_4)ClO_4] = 1 \times 10^{-1}$ M, V_0 = 1.70 mL. All spectra are corrected for dilution effects.

mode of Cl^- in **4** differs from the monodentate coordination encountered in $NiCl^+$.

Considering the high association constant K_{11} found for the uptake of the first F^- anion by receptor **4** (Table 2) and to further ascertain the large selectivity of receptor **4** for fluoride over chloride (i.e., log $K_{11}(F)$ − log $K_{11}(Cl) \approx 4$), we performed a competition experiment in which fluoride was added to the chlorido-bridged complex **6** (eq 3). Figure 6 shows the spectral changes that occur upon addition of $N(n\text{-}Bu)_4F$ to a ∼5 × 10^{-3} M solution of the chlorido-bridged complex **6**. Titrating fluoride into the solution induces a noticeable color change from green to pale green, due to a hypochromic shift of the ν_1 and ν_2 bands from 639 and 1037 nm to 624 and 1024 nm (at a 1:1 ratio), clearly evidencing the formation of substantial amounts of the fluorido-bridged complex **5**. Subsequent nonlinear least-squares refinement for a speciation model involving **5** and **6** provides an equilibrium constant of log K_{comp} = 4.2(1), which agrees well with the difference log $K_{11}(F)$ − log $K_{11}(Cl)$ found above. Thus, as established by direct titrations, the fluoride complex is ∼4 orders of magnitude more stable than the chlorido complex (Table 2).

Table 2. Equilibrium Constants for Halide Uptake by $[Ni_2(L^{Me2H4})]^{2+}$ (4)

anion	complex	log K_{11}	log K_{12}
F^-	$[Ni_2L(\mu\text{-}F)]^+$ (**5**)	7.77(9)[a]	4.54 (1)[a]
Cl^-	$[Ni_2L(\mu\text{-}Cl)]^+$ (**6**)	4.06(7)[a,b]	
Br^-	$[Ni_2L(\mu\text{-}Br)]^+$ (**7**)	2.01(1)[a]	
		5.38(1)[c]	3.87(1)[c]

[a]Solvent: MeCN/MeOH (1/1 v/v), T = 298(1) K. [b]Mean value of titrations in the UV and the visible. [c]Solvent: pure MeCN.

$$[Ni_2(L^{Me2H4})(\mu\text{-}Cl)]^+ + F^- \rightleftharpoons [Ni_2(L^{Me2H4})(\mu\text{-}F)]^+ + Cl^- \quad K_{comp} \qquad (3)$$

(**6** → **5**)

Figure 7 shows the changes in the vis−NIR region of the electronic absorption of a solution of $\mathbf{4}(ClO_4)_2$ in MeCN/MeOH (1/1 v/v) upon addition of a NH_4Br solution (Figure 7a) and in pure MeCN upon addition of $N(n\text{-}Bu)_4Br$ (Figure 7b). In the former case, the spectral perturbations are not so pronounced when compared with the F^- and Cl^- titrations. Thus, the intensity of the main absorption features of **4** decreases only slightly (by ∼10%), while at least one isosbestic point at 930 nm becomes visible.[45] A nonlinear least-squares refinement of the data set shown in Figure 7a returned a value of log K_{11} = 2.0(1) for the stability constant of the bromido complex **7**. In spite of a rather satisfactory fit, this value should however be taken as indicative rather than definitive given that at the end of the titration conversion reached only ∼50% with modest associated spectral changes. Unfortunately, **7**(Br)

DOI: 10.1021/acs.inorgchem.5b00123
Inorg. Chem. 2015, 54, 3937−3950

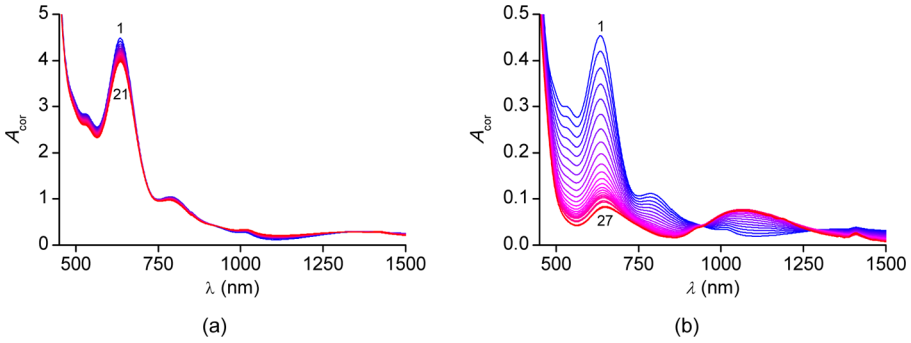

Figure 7. Spectrophotometric titration of the dinickel(II) complex $\mathbf{4}(ClO_4)_2$ as a function of increasing amounts of NH_4Br (a) or $N(n\text{-}Bu)_4Br$ (b) added in 25 μL increments. (a) Solvent: MeCN/MeOH (1/1 v/v), T = 298(1) K, $[\mathbf{4}(ClO_4)_2]_0 = 9.32 \times 10^{-3}$ M, $[NH_4Br] = 7 \times 10^{-2}$ M (spectra 1−21: 0−2.15 equiv), V_0 = 1.75 mL. (b) Solvent: MeCN, T = 298(1) K, $[\mathbf{4}(ClO_4)_2]_0 = 8.97 \times 10^{-4}$ M, $[N(n\text{-}Bu)_4Br] = 6.8 \times 10^{-3}$ M (spectra 1−21:0−2.23 equiv), $[N(n\text{-}Bu)_4Br] = 6.8 \times 10^{-2}$ M (spectra 22−27:4.98−33.45 equiv), supporting electrolyte $[N(n\text{-}Bu)_4ClO_4] = 1 \times 10^{-2}$ M, V_0 = 1.70 mL. All spectra are corrected for dilution effects.

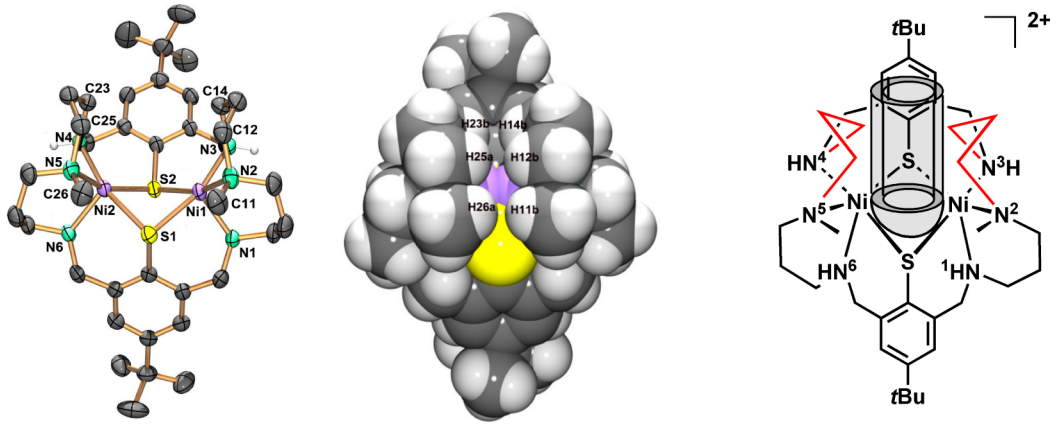

Figure 8. ORTEP (left) and space-filling representation (middle) of the molecular structure of the dicationic $[Ni_2(L^{Me2H4})]^{2+}$ receptor in crystals of $\mathbf{4}(ClO_4)_2\cdot 4EtOH$. Thermal ellipsoids are drawn at the 50% probability level. (right) Anion binding pocket of receptor **4**. The selectivity of **4** is essentially governed by the two opposing propylene linkers acting as a pair of jaws (highlighted in red).

precipitates at higher excesses of Br^- which prevented the titration to reach completion.

As mentioned earlier, complex **7**(Br) was found to be stable in neat acetonitrile. Indeed, the addition of $N(n\text{-}Bu)_4Br$ to **4** in MeCN (see Figure 7b) induced the spontaneous formation of bromido complex **7**, as clearly revealed by the hypochromic effect undergone by the $^3B_1 \rightarrow {}^3B_2$ absorption band centered at 635 nm, the concomitant disappearance of the $^3B_1 \rightarrow {}^3A_2$ band characteristic of **4**, the growing of a large feature at 1065 nm, and the presence of an apparent isosbestic point at 942 nm up to ~0.9 equiv. However, this point vanishes for higher amounts of $N(n\text{-}Bu)_4Br$, since the spectral morphology undergoes slight but discernible changes. The peak at 635 nm red-shifts by ~10 nm upon addition of 30 equiv of Br^- salt, while the intensity of the band at 1065 nm decreases, indicating the formation of a new species assumed to be a contact ion pair $[Ni_2(L^{Me2H4})(\mu\text{-}Br)]^+\cdots Br^-$ connected via a NH···Br^- bond. Indeed, a reasonable fit of the entire data set was only possible under consideration of two equilibria, yielding log K_{11} = 5.38(1) for $[Ni_2(L^{Me2H4})(\mu\text{-}Br)]^+$ and log K_{12} = 3.87(1) for $[Ni_2(L^{Me2H4})(\mu\text{-}Br)]^+\cdots Br^-$ (Supporting Information, Figures S11 and S12). Accordingly, the 1:1 inclusion complex reaches its maximal abundance (74%) upon addition of 1 equiv of bromide salt under the experimental titration conditions, whereas the molar fraction of the ion pair remains below 10% up to 0.8 equiv of Br^- (Supporting Information, Figure S13a), in agreement with the observation of an apparent isosbestic point at the beginning of the titration. It can be concluded that the bromido complex $[Ni_2(L^{Me2H4})(\mu\text{-}Br)]^+$ is 2 orders of magnitude more stable in acetonitrile than in methanol, and this most likely also holds for the fluorido and chlorido complexes. The close resemblance of the calculated electronic absorption spectra for both complexed species further supports the assignment of the 1:2 adduct to the $[Ni_2(L^{Me2H4})(\mu\text{-}Br)]^+\cdots Br^-$ hydrogen-bonded ion pair, as its formation is not expected to affect strongly the ligand field and thus the d−d transition energies (Supporting Information, Figure S13b).

X-ray Crystal Structure and Calculated Structure of Receptor 4. We employed X-ray crystallography and DFT calculations to gain insight into the factors that govern the anion selectivity. The crystal structure determination of the free receptor in crystals of $\mathbf{4}(ClO_4)_2\cdot 4EtOH$ showed the presence of a bowl-shaped $[Ni_2(L^{Me2H4})]^{2+}$ dication (Figure 8), comprising two distorted square-pyramidal Ni^{2+} ions (τ = 0.16).[46] Supporting Information, Table S1 lists selected bond lengths and angles. The two binding sites converge in a rather small anion binding-pocket of ~4 Å diameter formed by one aryl ring, two propylene chains (linking N3 and N2, and N4 and N5) and two NMe groups. The propylene groups appear to be orientated into the binding-pocket, filling the molecular void,[5] but the steric strain imposed by the macrocycle keeps them slightly above the van der Waals contact distances (H14b···

DOI: 10.1021/acs.inorgchem.5b00123
Inorg. Chem. 2015, 54, 3937−3950

H23b = 2.791 Å, H12b···H25a = 2.905 Å, H11b···H26a = 2.686 Å). The propylene chains presumably play a portal role in anion binding as detailed further below. Of note are also the Ni1−N2 and Ni2−N5 distances of 2.127(2) and 2.129(2) Å, which are elongated relative to those in $[Ni_2(L^{H6})]^{2+}$ (**1**, 2.069 and 2.070 Å, respectively),[17] indicative of a weaker ligand field of the tertiary amine donors as anticipated.[19,47]

Crystals of $\mathbf{4}(I)_2$·3*t*-BuOH·MeOH were obtained by slow evaporation of a solution of $\mathbf{4}(I)_2$ from a *t*-BuOH/MeOH (1/1 v/v) solution. The asymmetric unit comprises the free receptor **4**, two iodide counterions together with three *t*-BuOH, and one MeOH solvent molecules. The dications in $\mathbf{4}(I)_2$ (Supporting Information, Figure S14) and $\mathbf{4}(ClO_4)_2$ are isostructural, and the corresponding bond lengths and angles lie within narrow ranges. Thus, the iodides cannot fit in the binding cavity, as established by spectroscopy. However, the iodides are connected through NH···I$^-$ hydrogen bonds (N1···I1 = 3.632, N3···I1′′ = 3.641 Å) to the $[Ni_2(L^{Me2H4})]^{2+}$ cation.

The DFT (PBE0/TZV) optimized structure of **4** (Supporting Information, Figure S16) is close to that determined experimentally, although the calculated Ni−N and Ni−S distances are slightly larger than those observed in the crystal structure (Supporting Information, Table S1). The DFT orbital representation further reveals that both Ni d_{z^2} orbitals largely contribute to the lowest unoccupied molecular orbital (LUMO) and that they coincide with the binding site of the receptor.

X-ray Crystal Structures and Calculated Structures of the Fluorido, Chlorido, and Bromido Complexes 5−7. Crystals of $\mathbf{5}(F)$·5EtOH·2H_2O were obtained by slow evaporation of an ethanolic solution of $\mathbf{4}(ClO_4)_2$ containing 2 equiv of N(*n*-Bu)$_4$F. The formulation of the complex as a *fluorido* and not a *hydroxido* complex was confirmed by ESI-MS spectroscopy using the crystal that had been used for the crystallographic analysis (see Supporting Information). As can be seen, the fluorido ligand bridges the two Ni^{2+} ions (Figure 9). The Ni−F bond distances (2.046(2) and 2.078(2) Å) and

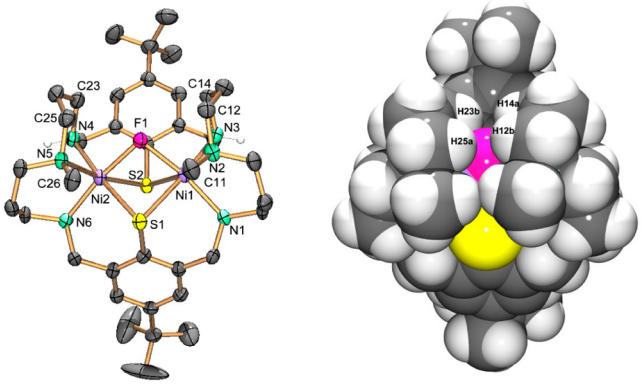

Figure 9. ORTEP (left) and space-filling representation (right) of the molecular structure of the fluorido complex $[Ni_2(L^{Me2H4})(\mu\text{-}F)]^+$ in crystals of $\mathbf{5}(F)$·5EtOH·2H_2O. Thermal ellipsoids are drawn at the 50% probability level.

the Ni−F−Ni angle (95.6°) are normal for Ni(μ-F)Ni bridges.[48] Notice the arrangement of the two propylene linkers that form a closed shell around the fluoride ion protecting it from the environment. The fluorido ligand is therefore not involved in H-bonding interactions with the surrounding H_2O and EtOH solvates. In other host−guest complexes, the halogenido ligands are more exposed to the medium; thus, the coordination spheres of intracavity halides are often completed by hydrogen-bonded solvate molecules.[5,49]

It is worth noting that the conformation of the macrocycle in host−guest complex **5** is virtually identical to that in the free receptor **4**. This is indicative of a high degree of preorganization. The structure also indicates that the host interacts with the fluorido ligand via six CH···F$^-$ hydrogen bonds[50] from the aliphatic CH_2 and CH_3 groups with C···F$^-$ distances in the range of 2.307−3.023 Å.

It is appropriate at this stage to comment on a possible "portal" role of the propylene groups. The propylene linkers create very narrow apertures of ca. 1.46 Å in **4** and 1.50 Å in **5**, as estimated from the average "cross" distances for H14a···H25a and H12b···H23b (3.86 Å in **4**, 3.90 Å in **5**) minus the sum (2.40 Å) of the van der Waals radii of two H atoms. This is too narrow to allow an unrestricted passage of a solvated fluoride anion (the naked anion having already a diameter of 2.57 Å)[51] into the receptor binding pocket (and vice versa). Thus, release and binding of the naked halide ion necessitates a movement of both propylene groups by ∼0.55 Å to widen the cavitand portal. It is likely that this movement involves a temporary lengthening of the Ni−N bonds involving the tertiary amine donors. The different host−guest behaviors of $[Ni_2(L^{H6})]^{2+}$ and $[Ni_2(L^{Me2H4})]^{2+}$, the latter of which has the longer (and thus weaker) Ni1−N2 and Ni2−N5 bonds, would be consistent with this view.

Crystals of the chlorido complex $\mathbf{6}(ClO_4)$·2EtOH·0.5MeOH were obtained by slow evaporation of $\mathbf{6}(ClO_4)$ from an ethanol/methanol (1/1 v/v) solution, while crystals of the bromido complex 7(Br)·2MeCN were grown from pure acetonitrile. The crystal structure determinations revealed the chlorido and bromido complexes (Figure 10) to be isostructural with the fluorido complex **5** (Figure 9). The corresponding bond lengths and angles within the $[Ni_2(L^{Me2H4})]^{2+}$ fragments are virtually identical. The average Ni−Cl (2.471(1) Å) and Ni−Br distances (2.646(1) Å), on the other hand, are significantly longer than the Ni−F (2.062 Å) distances as expected.[51]

The structures of **5**−**7** reveal that the Cl$^-$ and Br$^-$ ions fit less perfectly in the receptor binding cavity than the F$^-$ ion. This is particularly true if one compares the Ni−Hal distance differences across the series, that is, d(Ni−Cl) − d(Ni−F) = 0.41 Å versus d(Ni−Br) − d(Ni−Cl) = 0.18 Å. While the former value agrees reasonably well with the difference of the ionic radii of Cl$^-$ and F$^-$,[51] the latter is much larger than the predicted difference of 0.05 Å between Br$^-$ and Cl$^-$. The size fit mismatch of **4** for the heavier halide ions is further indicated by a pronounced increase of the C···C distances of the two opposing propylene groups upon going from F$^-$ to Br$^-$.[52] Consequently, the cavity entrances (estimated as described above for **4** and **5**) of 2.4 Å in **6** and 2.6 Å in **7** are much larger than in **4** and **5**. It is clear from the four structures that the macrocycle confers preorganization on the host which binds fluoride, chloride, and bromide via multiple Lewis acid−base interactions in a chelating manner.

The DFT-optimized structures of **5**−**7** at the PBE0/TZV level of theory are close to those determined by X-ray crystallography. For **5**, the calculated and experimental Ni−F and Ni−N mean distances match quite well, differing by only −0.0191 Å and −0.037 Å (Supporting Information, Table S1). The Ni−S computed distances are slightly longer than those found in the crystal structure (+0.079 Å). For **6** and **7**, the

DOI: 10.1021/acs.inorgchem.5b00123
Inorg. Chem. 2015, 54, 3937−3950

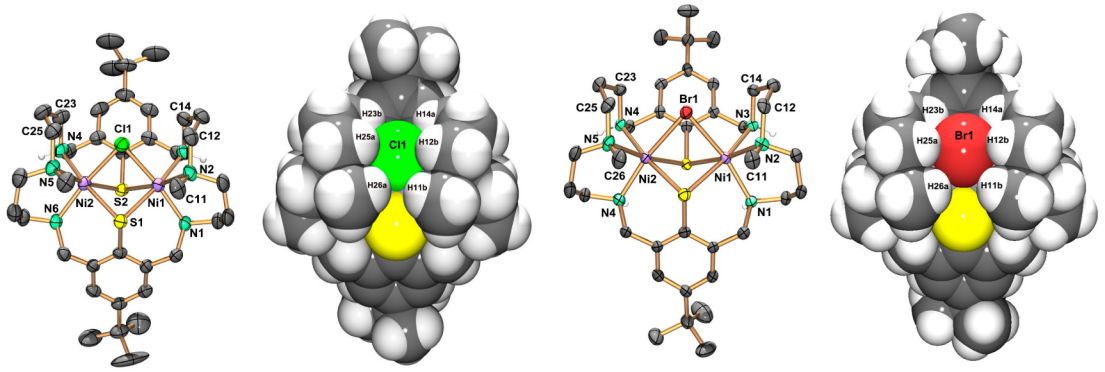

Figure 10. ORTEP and space-filling representations of the molecular structures of the chlorido and bromido complexes in crystals of **6**(ClO_4)·2EtOH·0.5MeOH (left) and **7**(Br)·2MeCN, respectively. Thermal ellipsoids are drawn at the 50% probability level.

calculated Ni−Cl (2.558 Å), Ni−Br (2.739 Å), and Ni−S bond lengths (2.577 and 2.583 Å) are slightly larger than those found in the solid state (differences ≤0.1 Å). The computed Ni−N bond distances are slightly shorter than those observed in the crystal. A good match is also seen in the Ni−Hal−Ni as well as in the Ni−S−Ni angles.

Calculated Structures of the Iodido-Bridged Complex $[Ni_2(L^{Me2H4})(\mu\text{-I})]^+$ (8) and Computed Stabilities of Halogenido-Bridged Complexes 5−8. Since the iodido-bridged complex $[Ni_2(L^{Me2H4})(\mu\text{-I})]^+$ (**8**) is synthetically inaccessible, we examined its structure by DFT calculations. The geometry optimizations for **8** were performed as for **5** and **7**, starting from the X-ray structure of the chlorido complex **6** and using the same level of theory. The optimized structure of the iodido complex was found to be isostructural with that of the other halogenido complexes **5**−**7**. Supporting Information, Table S1 lists selected bond lengths and angles.

A comparison of the structural features of the optimized structures of **5**−**8** reveals some striking features that may relate to the receptor anion selectivity. The first one concerns the increase of the Ni−Hal bond lengths. Thus, the increase by 1.003 Å of the Ni−Hal bond lengths upon going from F^- to I^- is significantly larger (by 0.088 Å) than the difference in the ionic radii of the free halide ions ($r(F^-) - r(I^-)$ = 0.915 Å),[51] suggesting that steric factors play a role. This is further supported by increasing structural distortions upon binding the heavier halides, as illustrated by the intermolecular distances between the facing pairs of carbon atoms of the two propylene chains at the cavity entrance. The C···C distances between pairs of facing atoms are very similar in case of complexes **4** (4.704 Å) and **5** (4.563 Å), indicating a good size match between the receptor **4** and the fluoride ion. Upon going to the heavier halides, the C···C distances increase substantially to 5.575 Å in the chlorido complex **6**, to 5.888 Å in the bromido complex **7**, and eventually reach 6.302 Å in the iodido complex **8**. Exactly the same trend was seen in the crystal structures.

To assess the magnitude of the host−guest interactions we also computed the affinities of receptor **4** for the four halide ions. The calculations were performed for the same medium (MeCN/MeOH 1/1 v/v) as the one used for the UV−vis−NIR spectrophotometric titrations (vide infra) to enable a validation of the computational approach by comparison with experimental data. The solution-phase affinities were calculated directly from the energy of the free receptor **4**, the corresponding halide ion, and respective host−guest complex. The optimized structures of **4**, host−guest complexes **5**−**8**, and the halide ions were subjected to single-point energy calculations using the PBE0 functional and a Def2-TVZ(P) basis set for all atoms. This method gave the following BSSE corrected affinities: $E_a(F^-)$ = 21.6 kcal/mol, $E_a(Cl^-)$ = 3.9 kcal/mol, $E_a(Br^-)$ = 0.8 kcal/mol, $E_a(I^-)$ = −6.4 kcal/mol. The values show that the fluorido complex **5** is substantially more stable than the chlorido complex **6**, while the bromido complex **7** is less stable than **6**, and the iodido complex **8** is unstable and therefore prone to spontaneous dissociation. These findings are in excellent agreement with the trend exhibited by the K_{11} binding constant values experimentally determined by UV−vis−NIR spectrophotometry and strongly support the hypothesis that the halide ion selectivity relates to a size fit mismatch of the receptor binding cavity for anions larger than F^- and increasing steric congestion of the host−guest system. This interpretation is further supported by the close resemblance of the UV−vis−NIR diffuse reflectance and absorption spectra of polycrystalline samples collected before and after dissolution, respectively.

■ CONCLUDING REMARKS

The main findings of the present work can be summarized as follows. (i) The dinuclear complex $[Ni_2(L^{Me2H4})]^{2+}$ (**4**) supported by the partially N-methylated N_6S_2 donor ligand H_2L^{Me2H4} exhibits a chelating $N_3Ni(\mu\text{-}S)_2NiN_3$ core with two square-pyramidal Ni^{2+} ions situated in an anion binding pocket of ∼4 Å diameter formed by the organic backbone of the $(L^{Me2H4})^{2-}$ macrocycle. (ii) The alkylation of the two *N*-methyl functions has a strong influence on the reactivity of the corresponding receptor **4**. Thus, in contrast to complex $[Ni_2(L^{H6})]^{2+}$ (**1**) supported by the parent H_2L^{H6} macrocycle, **4** reacts readily with fluoride, chloride (in MeCN/MeOH), and bromide ions (in MeCN) to afford the corresponding halogenido-bridged complexes $[Ni_2(L^{Me2H4})(\mu\text{-Hal})]^+$ **5**, **6**, and **7**. (iii) Receptor **4** binds only F^-, Cl^-, and Br^- anions in the same order of decreasing selectivity. With iodide or other polyatomic anions (ClO_4^-, NO_3^-, HCO_3^-, $H_2PO_4^-$, HSO_4^-, SO_4^{2-}) no reaction occurs. (iv) The binding events are accompanied by large and anion-specific UV−vis−NIR spectral changes, due to a change of both the coordination geometry of the divalent nickel ions from square-pyramidal (N_3S_2 donor set in **4**) to octahedral in the halogenido-bridged complexes (N_3S_2Hal donor environment in **5**−**7**) and the ligand-field strength upon F^- or Cl^- uptake. (v) The spectrophotometric titrations yielded the stability constants for the 1:1 complexes (K_{11}). The corresponding values found in MeCN/MeOH 1/1

DOI: 10.1021/acs.inorgchem.5b00123
Inorg. Chem. 2015, 54, 3937−3950

v/v decrease substantially from log K_{11} = 7.77(9) for the fluorido complex **5**, to 4.06(7) for the chlorido complex **6**, and to 2.0(1) for the bromido complex **7**. (vi) Receptor **4** has four secondary amine donor functions in the ligand periphery. These can engage in secondary NH···Hal$^-$ interactions to form adducts of 1:2 stoichiometry. The secondary NH···Hal$^-$ interactions are ∼3 orders of magnitude weaker than the Ni···Hal$^-$ bonds. (vii) The structures of the host−guest complexes **5**−**7** were ascertained by X-ray crystallography. The incapacity of receptor **4** to bind iodide ions was confirmed by the crystal structure of the salt **4**(I)$_2$. (viii) A comparison of the structures reveals a significant increase of the distance between the two propylene groups at the cavity entrance in case of Cl$^-$, Br$^-$, and I$^-$ (for the DFT-computed structure), while they are nearly identical in **4** and **5**. This further suggests a high degree of preorganization of the $[Ni_2(L^{Me2H4})]^{2+}$ receptor and a size fit mismatch of its binding cavity for anions larger than F$^-$. (ix) These results are substantiated by the DFT calculations. We are currently probing the possibility whether the anion binding selectivity of **4** can be further enhanced by properly fine-tuning of the supporting N_6S_2 macrocycle or by replacing Ni^{2+} by other metal ions.

EXPERIMENTAL SECTION

Materials and Methods. Compound **2** was prepared as described in the literature.[53] The synthesis of receptor **4**$(ClO_4)_2$ was performed under a protective atmosphere of argon. Melting points were determined in open-glass capillaries and are uncorrected. ESI mass spectra were recorded on a Bruker Daltronics APEX II spectrometer. NMR spectra were recorded on a Bruker AVANCE DPX-200 or a Bruker AVANCE DRX 400 spectrometer at 298 K. Chemical shifts refer to solvent signals. Mid (4000−400 cm^{-1}) and far (700−80 cm^{-1}) infrared spectra at 4 cm^{-1} resolution were recorded on Bruker TENSOR 27 (KBr pellets) and VERTEX70v (equipped with an A225 diamond ATR accessory from Bruker) FT-IR spectrometers, respectively. Solution absorption spectra were collected on a Jasco V-670 UV−vis−NIR spectrophotometer using 1 cm quartz cells (Hellma). Diffuse reflectance spectra of pure microcrystalline complexes were acquired between 200 and 2500 nm on a CARY 5000 (Agilent) UV−vis−NIR spectrophotometer fitted with a Praying Mantis accessory (Harrick), the baseline being recorded on dry barium sulfate (Avocado, <99%). Corrected reflectance data were converted to $f(R)$ values using the Kubelka−Munk function expressed as $f(R) = (1 - R)^2/2R$. Elemental analyses were performed on a vario EL elemental analyzer (Elementar Analysensysteme GmbH, Hanau). The room-temperature magnetic moments were measured for powdered solid samples using a MPMS 7XL SQUID magnetometer (Quantum Design) in an applied magnetic field of 1 T. The observed susceptibility data were corrected for underlying diamagnetism. ***CAUTION!*** *Although no problems were encountered during this work with the perchlorate salts, these compounds should be considered potentially explosive, be prepared only in small quantities, and handled with appropriate care.*

Compound 3. Solutions of 1,2-bis(4-*t*-butyl-2,6-diformylphenylthio)ethane **2** (2.00 g, 4.25 mmol) in dichloromethane (150 mL) and N^1-(3-aminopropyl)-N^1-methylpropane-1,3-diamine (1.23 g, 8.50 mmol) in ethanol (150 mL) were added simultaneously over a period of 5 h to a mixture of dichloromethane (300 mL) and ethanol (100 mL) at 0 °C. After complete addition, the reaction mixture was stirred at room temperature for 18 h. The dichloromethane was removed at reduced pressure, and sodium borohydride (1.29 g, 34.0 mmol) was added in small portions. After it was stirred at room temperature for 4 h, the reaction mixture was acidified to pH 1 with concentrated hydrochloric acid, and the resulting colorless suspension was evaporated to dryness. The residue was taken up in aqueous potassium hydroxide (3 M, 80 mL) and extracted with dichloromethane (4 × 80 mL). The combined organic fractions were dried with magnesium sulfate. Evaporation of the solvent gave **3** (2.88 g, 97%) as a colorless foamy solid. An analytical sample was obtained by recrystallization from ethanol. mp 47−49 °C. ^{1}H NMR (400 MHz, $CDCl_3$): δ = 1.32 (s, 18 H, C(CH_3)$_3$), 1.77 (m, 8 H, (NCH$_2$$CH_2CH_2$)$_2$N), 2.25 (s, 6 H, NC$H_3$), 2.46 (t, ^3J = 6.0 Hz, 8 H, (NCH$_2$CH$_2$$CH_2$)$_2$N), 2.82 (t, ^3J = 6.0 Hz, 8 H, (NCH_2CH$_2$CH$_2$)$_2$N), 3.17 (s, 4 H, (ArSCH_2)$_2$), 4.00 (s, 8 H, ArCH_2N), 7.41 (s, 4 H, Ar*H*). ^{13}C{^{1}H} NMR (100 MHz, $CDCl_3$): δ = 27.2 ($CH_2CH_2CH_2$), 31.2 (C(CH_3)$_3$), 34.7 ($C(CH_3)_3$), 37.3 ((ArSCH_2)$_2$), 42.9 (NCH_3), 48.6 ((NCH$_2$CH$_2$$CH_2$)$_2$N), 53.6 ((NCH$_2CH_2CH_2$)$_2$N), 56.0 (ArC$H_2$N), 126.2 (ArC-3, ArC-3′), 129.7 (ArC-1), 144.4 (ArC-2, ArC-2′), 152.2 (ArC-4). IR (KBr, cm^{-1}): $\tilde{\nu}$ = 3424 (m), 3280 (m, ν(NH)), 3049 (w), 2951 (s), 2864 (s), 2837 (s), 2792 (s), 1595 (m), 1560 (m), 1461 (s), 1407 (m), 1396 (m), 1362 (m), 1290 (w), 1262 (w), 1121 (m), 1202 (m), 1180 (m), 1134 (m), 1062 (w), 1047 (w), 925 (w), 881 (w), 732 (w). (+)-ESI-MS: m/z (CH_3CN) = 697.5 [M + H]$^+$. Anal. Calcd (%) for $C_{40}H_{68}N_6S_2$·EtOH (697.14 + 46.07): C 67.87, H 10.04, N 11.31; found: C 67.78, H 9.78, N 11.50. This compound was additionally characterized by X-ray crystallography (Supporting Information, Figure S15).

H_2L^{Me2H4}·6HBr. A solution of **3** (2.00 g, 2.9 mmol) in tetrahydrofuran (35 mL) was added dropwise to a solution of sodium (435 mg, 18.8 mmol) in liquid ammonia (100 mL). The resulting blue reaction mixture was stirred for further 4 h at −50 to −60 °C. Solid ammonium bromide (1.3 g, 13.0 mmol) was added to destroy the excess of the reducing agent. The resulting colorless suspension was allowed to warm to room temperature. After 12 h, the remaining solvent was distilled at reduced pressure. The residue was taken up in water (40 mL), and the solution was acidified to pH 1 with ∼4 mL of 48% hydrobromic acid. The solution was evaporated to dryness. Methanol (50 mL) was added, and the mixture was stirred for 3 d. The resulting solid was filtered, washed with methanol, and dried in vacuum. Yield: 2.14 g (64%), colorless solid. mp > 260 °C (decomposes without melting). ^{1}H NMR (300 MHz, D_2O): δ = 1.32 (s, 18 H, C(CH_3)$_3$), 2.15 (m, 8 H, (NCH$_2$$CH_2CH_2$)$_2$N), 2.97 (s, 6 H, N$CH_3$), 3.08 (t, ^3J = 7.5 Hz, 8 H, (NCH_2CH$_2$CH$_2$)$_2$N), 3.35 (*m*, 8 H, (NCH$_2$CH$_2$$CH_2$)$_2$N), 4.41 (s, 8 H, ArC$H_2$N), 7.63 (s, 4 H, Ar*H*). ^{13}C{^{1}H} NMR (75 MHz, D_2O): δ = 21.1 ($CH_2CH_2CH_2$), 30.5 (C(CH_3)$_3$), 34.2 ($C(CH_3)_3$), 40.5 (NCH_3), 43.5 ((NCH$_2$CH$_2$CH$_2$)$_2$N), 51.3 (ArCH_2N), 52.8 ((NCH$_2$CH$_2$CH$_2$)$_2$N), 130.3 (ArC-3, ArC-3′), 134.1 (ArC-1), 133.6 (ArC-2, ArC-2′), 150.8 (ArC-4). IR (KBr, cm^{-1}): $\tilde{\nu}$ = 3424 (s), 2957 (s), 2739 (s), 2392 (m), 1635 (m), 1623 (m), 1576 (m), 1559 (m), 1458 (s), 1413 (m), 1367 (w), 1233 (w), 1208 (w), 1163 (w), 1052 (w), 996 (w), 927 (w), 896 (w), 755 (w), 736 (w), 539 (w). (+)-ESI-MS: m/z (MeOH) = 671.49 [M + H]$^+$, 751.41 [M+H+HBr]$^+$, 336.25 [M+2H]$^{2+}$. Anal. Calcd (%) for $C_{38}H_{66}N_6S_2$·6HBr·H_2O (671.10 + 485.47 + 18.01): C 38.86, H 6.35, N 7.15, Br 40.82; found: C 38.69, H 6.39, N 7.10, Br 40.47.

[Ni$_2$(L^{Me2H4})](ClO$_4$)$_2$ (4(ClO$_4$)$_2$). To a suspension of H_2L^{Me2H4}·6HBr (500 mg, 0.43 mmol) in MeOH (50 mL) was added Ni(CH$_3$CO$_2$)$_2$·4H$_2$O (215 mg, 0.86 mmol) in MeOH (5 mL), followed by triethylamine (485 mL, 3.44 mmol) dissolved in MeOH (2 mL). The resulting dark green solution was stirred for 3 h, then $LiClO_4$·3H$_2$O (700 mg, 4.37 mmol) was added, while stirring was maintained for another 3 h. The resulting solid was filtered and washed with ethanol, and the crude product was purified by recrystallization from a mixed acetonitrile/ethanol solution. Yield: 0.286 g (67%). mp > 317 °C (decomposes without melting). IR (KBr, cm^{-1}): $\tilde{\nu}$ = 3442 (s), 3282 (m), 2953 (s), 2867 (s), 1629 (m), 1460 (s), 1363 (m), 1297 (w), 1229 (w), 1186 (w), 1121 (s, ν(ClO_4^-)), 1108 (s, ν(ClO_4^-)), 1050 (s, ν(ClO_4^-)), 977(m), 945 (w), 873 (m), 815 (w), 744 (w), 675 (w), 625 (s, ν(ClO_4^-)). Anal. calcd (%) for $C_{38}H_{64}Cl_2N_6Ni_2O_8S_2$·2H$_2$O (985.37 + 36.03): C 44.68, H 6.71, N 8.23; found: C 44.91, H 6.23, N 8.21. Magnetic moment: $\mu_{eff,dim}$ = 4.33 μ_B (per binuclear unit), μ_{eff} = 3.06 μ_B (per Ni^{2+}).

[Ni$_2$(L^{Me2H4})](I)$_2$ (4(I)$_2$). To a solution of **4**$(ClO_4)_2$ (98.5 mg, 0.10 mmol) in acetonitrile (30 mL) was added with stirring a solution of N(n-Bu)$_4$I (369 mg, 1.00 mmol) in acetonitrile (5 mL) at room temperature. The reaction mixture was stirred for ∼1 h, after which

DOI: 10.1021/acs.inorgchem.5b00123
Inorg. Chem. 2015, 54, 3937−3950

dark green crystals formed. The crude product was filtered and purified by recrystallization from a mixed methanol/ethanol solution. Yield: 50 mg (53%). mp >208 °C (decomposes without melting). IR (KBr, cm^{-1}): $\tilde{\nu}$ = 3420 (m), 3124 (m), 2950 (s), 2906 (s), 2861 (s), 1619 (w), 1460 (s), 1362 (m), 1296 (w), 1225 (w), 1185 (w), 1158 (s), 1089 (m), 1050 (s), 979 (m), 947 (w), 873 (m), 847 (w), 815 (w), 752 (w), 675 (w), 630 (w), 501 (w). Magnetic moment: $\mu_{eff,dim}$ = 4.63 μ_B (per binuclear unit), μ_{eff} = 3.27 μ_B (per Ni^{2+}). Anal. calcd (%) for $C_{38}H_{64}I_2N_6Ni_2S_2{\cdot}2H_2O$ (1040.28 + 36.03): C 42.40, H 6.37, N 7.81; found: C 41.75, H 6.34, N 7.55. Crystals of **4**$(I)_2{\cdot}3t$-BuOH·MeOH suitable for X-ray crystallography were obtained by slow evaporation of a mixed *t*-BuOH/MeOH solvent system.

[$Ni_2(L^{Me2H4})(\mu$-F)](ClO$_4$) (5(ClO$_4$)). To a solution of **4**$(ClO_4)_2$ (98.5 mg, 0.10 mmol) in acetonitrile (30 mL) was added a solution of N(*n*-Bu)$_4$F·3H$_2$O (47.3 mg, 0.15 mmol) in acetonitrile (5 mL) at room temperature, resulting in an immediate color change from dark green to bright green. The reaction mixture was stirred for ∼10 min, after which a solution of $LiClO_4{\cdot}3H_2O$ (160 mg, 1.00 mmol) in ethanol (5 mL) was added. The solution was concentrated under reduced pressure until bright green crystals formed, which were filtered, washed with cold ethanol, and dried in vacuum. The crude product was purified by recrystallization from a mixed acetonitrile/ethanol solution. Yield: 78 mg (86%). mp > 217 °C (decomposes without melting). IR (KBr, cm^{-1}): $\tilde{\nu}$ = 3445 (m), 3275 (m), 2953 (s), 2923 (s), 2861 (s), 1625 (w), 1446 (s), 1392 (w), 1362 (m), 1299 (w), 1280 (w), 1227 (w), 1188 (w), 1157 (m), 1082 (s), 978 (m), 922 (w), 869 (m), 815 (w), 745 (w), 671 (w), 623 (m), 549 (w), 497 (w). Magnetic moment: $\mu_{eff,dim}$ = 4.30 μ_B (per binuclear unit), μ_{eff} = 3.03 μ_B (per Ni^{2+}). Anal. calcd (%) for $C_{38}H_{64}ClFN_6Ni_2O_4S_2{\cdot}2H_2O$ (904.2 + 36.03): C 48.50, H 7.28, N 8.95; found: C 48.24, H 7.21, N 8.63. Crystals of **5**(F)·5EtOH·2H$_2$O were obtained by slow evaporation of an ethanolic solution of **4**$(ClO_4)_2$ to which 2 equiv of N(*n*-Bu)$_4$F were added.

[$Ni_2(L^{Me2H4})(\mu$-Cl)](ClO$_4$) (6(ClO$_4$)). To a colorless suspension of $H_2L^{Me2H4}{\cdot}6HBr$ (0.500 g, 0.430 mmol) in methanol (50 mL) was added 860 μL of a 1 M solution of $NiCl_2{\cdot}6H_2O$ (0.86 mmol) in methanol (5 mL) followed by a solution of triethylamine (485 μL, 3.46 mmol) dissolved in MeOH. After this suspension was stirred for 3 h at room temperature, a solution of $LiClO_4{\cdot}3H_2O$ (700 mg, 4.37 mmol) in ethanol (5 mL) was added. The solution was concentrated in vacuum to half of its original volume to give a green solid, which was filtered and washed with cold ethanol. The crude product was purified by slow evaporation of a mixed acetonitrile/ethanol solution. Yield: 0.220 g (56%). mp > 289 °C (decomposes without melting). IR (KBr, cm^{-1}): $\tilde{\nu}$ = 3441 (s), 3288 (m), 3267 (m), 2952 (s), 2926 (m), 2906 (m), 2862 (s), 2815 (m), 2023 (w), 1628 (m), 1462 (s), 1394 (w), 1379 (w), 1363 (m), 1299 (w), 1283 (w), 1272 (w), 1238 (w), 1227 (w), 1188 (w), 1157 (m), 1122 (s, $\nu(ClO_4^-)$), 1109 (s, $\nu(ClO_4^-)$), 1090 (s, $\nu(ClO_4^-)$), 1064 (s, $\nu(ClO_4^-)$), 1051 (s, $\nu(ClO_4^-)$), 1017 (w), 1005 (w), 977 (m), 954 (w), 941(w), 921 (w), 872 (m), 815 (m), 755 (w), 745 (m), 673 (w), 636 (s, $\nu(ClO_4^-)$), 625 (s, $\nu(ClO_4^-)$), 549 (w), 497 (w), 413 (w). Magnetic moment: $\mu_{eff,dim}$ = 4.65 μ_B (per binuclear unit), μ_{eff} = 3.29 μ_B (per Ni^{2+}). Anal. calcd (%) for $C_{38}H_{64}Cl_2Ni_2N_6O_4S_2$ (921.38): C 49.54, H 7.00, N 9.12; found: C 49.05, H 7.11, N 9.01. Crystals of **6**$(ClO_4){\cdot}2$EtOH·0.5MeOH suitable for X-ray crystallography were obtained by slow evaporation of a mixed methanol/ethanol (1/1 v/v) solution of **5**(ClO_4). The crystals quickly lose the solvate molecules upon standing in air and turn dull.

[$Ni_2(L^{Me2H4})(\mu$-Br)](Br) (7(Br)). To a solution of **4**$(ClO_4)_2$ (98.5 mg, 0.10 mmol) in acetonitrile (30 mL) was added with stirring a solution of N(*n*-Bu)$_4$Br (322 mg, 1.00 mmol) in acetonitrile (5 mL) at room temperature. The reaction mixture was stirred for ∼1 h, after which the title compound precipitated as bright green crystals. The product was filtered and purified by recrystallization from acetonitrile. Yield: 67 mg (64%). mp > 223 °C (decomposes without melting). IR (KBr, cm^{-1}): $\tilde{\nu}$ = 3406 (m), 3195 (m), 2953 (s), 2859 (s), 1621 (w), 1460 (s), 1360 (m), 1299 (w), 1271 (w), 1226 (w), 1188 (w), 1159 (m), 1091 (m), 1050 (s), 976 (m), 920 (w), 873 (m), 743 (m), 673 (w), 631 (w), 553 (w), 495 (w). Magnetic moment: $\mu_{eff,dim}$ = 4.60 μ_B (per binuclear unit), μ_{eff} = 3.25 μ_B (per Ni^{2+}). Anal. calcd (%) for $C_{38}H_{64}Br_2N_6Ni_2S_2{\cdot}2H_2O$ (946.28 + 36.03): C 46.46, H 6.98, N 8.56; found: C 46.61, H 7.00, N 8.72.

Crystallography. The data sets for **3**·0.5EtOH, **4**$(ClO_4)_2{\cdot}4$EtOH, **4**$(I)_2{\cdot}3t$-BuOH·MeOH, **5**(F)·5EtOH·2H$_2$O, **6**$(ClO_4){\cdot}2$EtOH·0.5MeOH, and **7**(Br)·2MeCN were collected using a STOE IPDS-2T diffractometer equipped with graphite monochromated Mo Kα radiation (0.710 73 Å). The intensity data were processed with the program STOE X-AREA.[54] Structures were solved by direct methods[55] and refined by full-matrix least-squares on the basis of all data against F^2 using SHELXL-97.[56] PLATON was used to search for higher symmetry.[57] Default values for van der Waals radii as implemented in ORTEP3 for Windows were used for the space-filling representations.[58] H atoms were placed at calculated positions and refined as riding atoms with isotropic displacement parameters. All non-hydrogen atoms were refined anisotropically. Additional crystallographic information is available in the Supporting Information.

Crystal Data for 3·0.5EtOH. $C_{41}H_{71}N_6O_{0.50}S_2$, M = 720.16 g/mol, triclinic space group $P\bar{1}$, a = 5.906(1), b = 13.585(3), c = 26.661(5) Å, α = 84.44(3), β = 85.88(3), γ = 81.51(3)°, V = 2102.2(7) Å^3, Z = 2, D_c = 1.138 g/cm^3, μ = 0.163 mm^{-1}, 15 758 reflections collected, 7322 unique (R_{int} = 0.0951). Final R_1 [$F^2 > 2\sigma(F^2)$] = 0.0750, wR_2 (all data) = 0.2094, R_1 index based on 3173 reflections with $I > 2\sigma(I)$ (refinement on F^2). The ethanol solvate molecule is situated in the vicinity of an inversion center.

Crystal Data for 4(ClO$_4$)$_2$·4EtOH. $C_{38}H_{64}Cl_2N_6Ni_2O_8S_2(EtOH)_4$, M = 985.39 + 184.2 g/mol, triclinic space group $P\bar{1}$, a = 13.956(3), b = 16.397(3), c = 23.670(5) Å, α = 84.64(3), β = 81.11(3), γ = 82.13(3)°, V = 5287(2) Å^3, Z = 4 (two crystallographically independent but chemically identical molecules A and B in the asymmetric unit), D_c = 1.227 g/cm^3, μ = 0.939 mm^{-1}, 59 120 reflections collected, 28 392 unique (R_{int} = 0.0441). Final R_1 [$F^2 > 2\sigma(F^2)$] = 0.0475, wR_2 (all data) = 0.1311, R_1 index based on 18 013 reflections with $I > 2\sigma(I)$ (refinement on F^2). In the crystal structure of **4**$(ClO_4)_2{\cdot}4$EtOH, the four ethanol molecules are heavily disordered and were therefore removed from the structure (and the corresponding F_0) with the SQUEEZE procedure implemented in the PLATON program suite.[57] Removing the four ethanol molecules led to two solvent-accessible voids of 552 and 575 Å^3, in good agreement with the space needed by four ethanol molecules. Two ClO_4^- ions were found to be disordered over two positions. Split atom models using SADI instructions implemented in SHELXL were applied to account for this disorder. The site occupancies of the respective orientations were fixed or refined as follows: O(1a)−O(4a)/O(1b)−O(4b) = 0.68(1)/0.32(1), and O(13a)−O(16a)/O(13b)−O(16b) = 0.77(1)/0.23(1).

Crystal Data for 4(I)$_2$·3t-BuOH·MeOH. $C_{38}H_{64}I_2N_6Ni_2S_2(t\text{-}BuOH)_3(MeOH)$, M = 1040.28 + 254.41 g/mol, orthorhombic space group *Pnma*, a = 10.976(2), b = 20.089(4), c = 27.435(6) Å, V = 6049(2) Å^3, Z = 4 (the asymmetric unit contains half of the formula unit), D_c = 1.422 g/cm^3, μ = 1.756 mm^{-1}, 56 201 reflections collected, 7506 unique (R_{int} = 0.0560). Final R_1 [$F^2 > 2\sigma(F^2)$] = 0.0536, wR_2 (all data) = 0.1105, R_1 index based on 5704 reflections with $I > 2\sigma(I)$ (refinement on F^2). One of the *t*-BuOH molecules and the two *t*-Bu groups of the supporting ligand were found to be disordered over two positions. Split atom models using SADI instructions implemented in SHELXL were applied to account for this disorder. The site occupancies were fixed at 0.50/0.50.

Crystal Data for 5(F)·5EtOH·2H$_2$O. $C_{48}H_{98}F_2N_6Ni_2O_7S_2$, M = 1090.86 g/mol, monoclinic space group $P2_1/n$, a = 14.250(5), b = 16.805(5), c = 24.438(5) Å, β = 99.969(5)°, V = 5764(3) Å^3, Z = 4, D_c = 1.257 g/cm^3, μ = 0.782 mm^{-1}, 35 994 reflections collected, 12 691 unique (R_{int} = 0.1012). Final R_1 [$F^2 > 2\sigma(F^2)$] = 0.0591, wR_2 (all data) = 0.1288, R_1 index based on 5535 reflections with $I > 2\sigma(I)$ (refinement on F^2). One EtOH solvate molecule was found to be disordered over two positions. The site occupancies of the respective orientations were refined as follows: O(6), C(45), C(46a)/O(6), C(45), C(46b) = 0.57(2)/0.43(2).

Crystal Data for 6(ClO$_4$)·2EtOH·0.5MeOH. $C_{42.5}H_{78}Cl_2N_6Ni_2O_{6.5}S_2$, M = 1029.55 g/mol, monoclinic space group $P2_1/c$, a = 17.101(3), b = 22.759(5), c = 14.379(3) Å, β = 102.60(3)°, V = 5461.7(2) Å^3, Z = 4, D_c = 1.252 g/cm^3, μ = 0.910

DOI: 10.1021/acs.inorgchem.5b00123
Inorg. Chem. 2015, 54, 3937−3950

mm^{-1}, 45 132 reflections collected, 9269 unique (R_{int} = 0.0476). Final R_1 [$F^2 > 2\sigma(F^2)$] = 0.0495, wR_2 (all data) = 0.1347, R_1 index based on 5369 reflections with $I > 2\sigma(I)$ (refinement on F^2). One *t*-Bu group was found to be disordered over two positions. Split atom models using SADI instructions implemented in SHELXL were applied to account for this disorder. The site occupancies were refined (C36a-C38a/C36b-C38b = 0.78/0.22).

Crystal Data for 7(Br)·2MeCN. $C_{38}H_{64}Br_2N_6Ni_2S_2(MeCN)_2$, M = 946.28 + 82.10 g/mol, monoclinic space group $P2_1/c$, a = 16.169(3), b = 20.949(4), c = 27.792(6) Å, β = 91.85(2)°, V = 9409(3) Å^3, Z = 8 (the asymmetric unit contains two formula units), D_c = 1.452 g/cm^3, μ = 2.626 mm^{-1}, 54 973 reflections collected, 22 338 unique (R_{int} = 0.0701). Final R_1 [$F^2 > 2\sigma(F^2)$] = 0.0800, wR_2 (all data) = 0.2011, R_1 index based on 14 327 reflections with $I > 2\sigma(I)$ (refinement on F^2). Two MeCN solvate molecules were found to be disordered over two positions. Split atom models using SADI instructions implemented in SHELXL were applied to account for this disorder. The site occupancies were fixed at 0.50/0.50.

Spectrophotometric Titrations. All mother solutions were prepared by dissolving carefully weighted (balance accuracy: ± 0.1 mg) materials in an acetonitrile/methanol (1/1 v/v) HPLC-grade solvent mixture or in pure acetonitrile (VWR BDH Prolabo, HiPerSolv CHROMANORM). The titrations were performed in a MeCN/MeOH (1/1 v/v) solvent mixture, because the binding constants in MeCN (for **5** and **6**) were found to be too high to be measured directly by spectrophotometry. They were performed in a quartz cell (Hellma 110-QS) of 1 cm optical path length containing 1.7 or 1.75 mL of a dinickel(II) complex stock solution by manual addition of 25 μL aliquots of the corresponding halide salts (NH_4Cl, NH_4Br, N(*n*-Bu)$_4$F·3H$_2$O, N(*n*-Bu)$_4$Br) with an Eppendorf micropipette (volume range of 10−100 μL; 3.0−0.8% error). UV−vis−NIR absorption spectra were collected in the 190−450 and 450−1500 nm ranges at uniform data point intervals of 1 nm with a double-beam V-670 (Jasco) spectrophotometer, which is certified by the manufacturer to have a linear response up to 6 AU. Moreover, it was ascertained that solutions of the $[Ni_2(L^{Me2H4})](ClO_4)_2$ complex obey the Lambert−Beer law up to 1 × 10^{-2} M. Equilibration time between each incremental addition was found to be fast, as identical spectra were obtained by cycling the recordings with a 4 min delay between two consecutive measurements.

The multiwavelength data sets were decomposed in their principal components by factor analysis before refining the apparent equilibrium constants and extinction coefficients by a nonlinear least-squares procedure implemented in the Specfit program.[37] Alternatively, the same data sets were analyzed by the HypSpec 2014 software,[39] which returned rigorously the same values as Specfit for a given chemical model. The goodness-of-fit was assessed by the standard deviation of the fit (σ), the visual inspection of the residuals, and by the physical meaning of the calculated electronic absorption spectra. Unless otherwise noted (standard deviation on the arithmetic mean), the reported uncertainties correspond to the standard deviation of the refined parameters that were returned by the fitting software. Distribution diagrams were generated with the Hyss program.[59]

Theoretical Calculations. Geometry optimizations were performed using DFT calculations based on the generalized gradient approximation of Perdew, Burke, and Ernzerhof (PBE0)[60,61] for the exchange and correlation functional[62] as implemented in the ORCA program package (version 2.8).[63,64] The triple-ζ valence basis set TZV was used for all atoms.[65] Frequency calculations were performed on the optimized structures of each compound to rule out the presence of any imaginary frequencies. To calculate the halide ion affinity, the PBE0/TZV optimized structures were subjected to single-point energy calculations using the PBE0/TZV(P) level of theory. The COSMO model[66] with a 1/1 mixture of MeCN/MeOH was used to account for solvent effects in all the calculations. The dielectric constant of the mixture was set to 34.6, assuming ε(mixture) = (ε(MeOH) + ε(MeCN))/2 with ε(MeOH) = 32.7 and ε(MeCN) = 37.5. The refractive index was set to 1.34. Relativistic effects were incorporated in all calculations.[67] The halide ion affinity E_a(Hal = F^-, Cl^-, Br^-, I^-) was calculated according to eq 5, where $^{HS}E([Ni_2(L^{Me2H4})(\mu\text{-Hal})]^+)$ represents the total energy of the respective halide complex in its high-spin state (Hal = F^- (**5**), Cl^- (**6**), Br^- (**7**), I^- (**8**)), ^{BS}E(**4**) the total energy of the free receptor (low-spin state), and E(Hal) the total energy of the halide ion.

$$[Ni_2(L^{Me2H4})]^{2+} + Hal \rightarrow [Ni_2(L^{Me2H4})(\mu\text{-Hal})]^+$$
$$\mathbf{4} \quad (Hal = F^-, Cl^-, Br^-, I^-) \quad (\mathbf{5}, \mathbf{6}, \mathbf{7}, \mathbf{8}) \qquad (4)$$

$$E_a(Hal) = {}^{HS}E([Ni_2(L^{Me2H4})(\mu\text{-Hal})]^+) - {}^{BS}E(\mathbf{4}) - E(Hal) \qquad (5)$$

■ ASSOCIATED CONTENT

Supporting Information

Proposed structure of the contact ion pair $[Ni_2(L^{Me2H4})(\mu\text{-F})]^+\cdots F^-$. Perspective views of the complexes **5**(F)·5EtOH·2H$_2$O and **7**(Br)·2MeCN showing intermolecular hydrogen bonding interactions. Spectrophotometric titrations of **4**(ClO$_4$)$_2$ with N(*n*-Bu)$_4$F, N(*n*-Bu)$_4$Cl, and N(*n*-Bu)$_4$Br in MeCN/MeOH 1/1 v/v, of **4**(ClO$_4$)$_2$ with N(*n*-Bu)$_4$Br in MeCN. Perspective views of the cation **4** in **4**(I$_2$)·3*t*-BuOH·MeOH and of proligand **3**. DFT orbital picture of the free receptor $[Ni_2(L^{Me2H4})]^{2+}$. Table of selected bond lengths and angles for **4**−**8**. Electrospray ionization mass spectra, UV−vis−NIR diffuse reflectance, and FT-FIR spectra of **4**(ClO$_4$)$_2$, **4**(I)$_2$, **5**(ClO$_4$), **6**(ClO$_4$), and **7**(Br). Calculation of halide ion affinities in the gas phase and in different solvents. Crystallographic data for proligand **3**·0.5EtOH, complexes **4**(ClO$_4$)$_2$·4EtOH, **4**(I)$_2$·3*t*-BuOH·MeOH, **5**(F)·5EtOH·2H$_2$O, **6**(ClO$_4$)·2EtOH·0.5MeOH, and **7**(Br)·2MeCN in cif format. This material is available free of charge via the Internet at http://pubs.acs.org. CCDC-917925 (**3**·0.5EtOH), CCDC-915779 (**4**(ClO$_4$)·4EtOH), CCDC-966355 (**4**(I)$_2$·3*t*-BuOH·MeOH), CCDC-966356 (**5**(F)·5EtOH·2H$_2$O), CDDC-915780 (**6**(ClO$_4$)·2EtOH·0.5MeOH), and CCDC-966357 (**7**(Br)·2MeCN) contain the supplementary crystallographic data for this paper. These data can be obtained free of charge from The Cambridge Crystallographic Data Centre via www.ccdc.cam.ac.uk/data_request/cif.

■ AUTHOR INFORMATION

Corresponding Authors

*E-mail: b.kersting@uni-leipzig.de. Fax: +49/(0)341-97-36199. (B.K.)

*E-mail: Michel.Meyer@u-bourgogne.fr. (M.M.)

Notes

The authors declare no competing financial interest.

■ ACKNOWLEDGMENTS

We are thankful to Prof. Dr. H. Krautscheid for providing facilities for X-ray crystallographic measurements. This work was supported by the Deutsche Forschungsgemeinschaft (Graduate School "BuildMona"), the Centre National de la Recherche Scientifique (CNRS), and the Conseil Régional de Bourgogne (PARI II-CDEA program).

■ REFERENCES

(1) Park, C. H.; Simmons, H. E. *J. Am. Chem. Soc.* **1968**, *90*, 2431−2432.

(2) Graf, E.; Lehn, J.-M. *J. Am. Chem. Soc.* **1976**, *98*, 6403−6405.

(3) For comprehensive reviews on anion recognition and design of anion receptors, see: (a) *Supramolecular Chemistry of Anions;* Bianchi, A., Bowman-James, K., García-España, E., Eds.; Wiley-VCH: New York, 1997. (b) Schmidtchen, F. P. *Coord. Chem. Rev.* **2006**, *250*,

DOI: 10.1021/acs.inorgchem.5b00123
Inorg. Chem. 2015, 54, 3937−3950

2918−2928. (c) Sessler, J. L.; Gale, P. A.; Cho, W. S. *Anion Receptor Chemistry;* RSC Publishing: Cambridge, U.K., 2006.
(4) Steed, J. W.; Atwood, J. L. *Supramolecular Chemistry,* 2nd ed.; J. Wiley & Sons: Chichester, U.K., 2009.
(5) Wallace, K. J.; Belcher, W. J.; Turner, D. R.; Syed, K. F.; Steed, J. W. *J. Am. Chem. Soc.* **2003**, *125*, 9699−9715.
(6) (a) Snowden, T. S.; Anslyn, E. V. *Curr. Opin. Chem. Biol.* **1999**, *3*, 740−746. (b) Martinez-Manez, R.; Sancenon, F. *Chem. Rev.* **2003**, *103*, 4419−4476. (c) Kubo, Y.; Yamamoto, M.; Ikeda, M.; Takeuchi, M.; Shinkai, S.; Yamaguchi, S.; Tamao, K. *Angew. Chem.* **2003**, *115*, 2082−2086; *Angew. Chem., Int. Ed.* **2003**, *42*, 2036−2040.
(7) Ilioudis, C. A.; Georganopoulou, D. G.; Steed, J. W. *CrystEngComm* **2002**, *4*, 26−36.
(8) (a) Hossain, A.; Liljegren, J. A.; Powell, D.; Bowman-James, K. *Inorg. Chem.* **2004**, *43*, 3751−3755. (b) Sarwar, M. G.; Dragisic, B.; Sagoo, S.; Taylor, M. S. *Angew. Chem.* **2010**, *122*, 1718−1721; *Angew. Chem., Int. Ed.* **2010**, *49*, 1674−1677.
(9) Shriver, D. F.; Biallas, M. J. *J. Am. Chem. Soc.* **1967**, *89*, 1078−1081.
(10) (a) Wedge, T. J.; Hawthorne, M. F. *Coord. Chem. Rev.* **2003**, *240*, 111−128. (b) Wade, C. R.; Broomsgrove, A. E. J.; Aldrige, S.; Gabbaï, F. P. *Chem. Rev.* **2010**, *110*, 3958−3984.
(11) Drew, M. G. B.; McCann, M.; Nelson, S. M. *J. Chem. Soc., Chem. Commun.* **1979**, 481−482.
(12) (a) Motekaitis, R. J.; Martell, A. E.; Murase, I. *Inorg. Chem.* **1986**, *25*, 938−944. (b) Motekaitis, R. J.; Martell, A. E. *Inorg. Chem.* **1991**, *30*, 694−700.
(13) (a) Amendola, V.; Bastianello, E.; Fabbrizzi, L.; Mangano, C.; Pallavicini, P.; Perotti, A.; Lanfredi, A. M.; Ugozzoli, F. *Angew. Chem.* **2000**, *112*, 3039−3042; *Angew. Chem., Int. Ed.* **2000**, *39*, 2917−2920. (b) Amendola, V.; Fabbrizzi, L.; Mangano, C.; Pallavicini, P.; Zema, M. *Inorg. Chim. Acta* **2002**, *337*, 70−74.
(14) Lehaire, M.-L.; Scopelliti, R.; Piotrowski, H.; Severin, K. *Angew. Chem.* **2002**, *114*, 1477−1480; *Angew. Chem., Int. Ed.* **2002**, *41*, 1419−1422.
(15) Frischmann, P.; MacLachlan, M. J. *Chem. Soc. Rev.* **2013**, *42*, 871−890.
(16) (a) Lenthall, J. T.; Steed, J. W. *Coord. Chem. Rev.* **2007**, *251*, 1747−1760. (b) Mezei, G.; Zaleski, C. M.; Pecoraro, V. L. *Chem. Rev.* **2007**, *107*, 4933−5003. (c) Garon, C. N.; Gorelsky, S. I.; Sigouin, O.; Woo, T. K.; Fontaine, F.-G. *Inorg. Chem.* **2009**, *48*, 1699−1710. (d) Núñez, C.; Bastida, R.; Macías, A.; Valencia, L.; Ribas, J.; Capelo, J. L.; Lodeiro, C. *Dalton Trans.* **2010**, *39*, 7673−7683.
(17) Lehmann, U.; Lach, J.; Loose, C.; Kortus, J.; Kersting, B. *Dalton Trans.* **2013**, *42*, 987−996.
(18) (a) Lozan, V.; Loose, C.; Kortus, J.; Kersting, B. *Coord. Chem. Rev.* **2009**, *253*, 2244−2260. (b) Kersting, B.; Lehmann, U. *Adv. Inorg. Chem.* **2009**, *61*, 407−470.
(19) Kersting, B.; Steinfeld, G. *Chem. Commun.* **2001**, 1376−1377.
(20) Ni^{2+} is a borderline case in terms of its Lewis-acidity and has an affinity for all halide ions: Huheey, J.; Keiter, E.; Keiter, R. *Anorganische Chemie,* 2nd ed.; de Gruyter: Berlin, Germany, 1995; p 400.
(21) For octahedral Ni complexes coligated with Br^- ligands, see: (a) Ito, T.; Kato, M.; Ito, H. *Bull. Chem. Soc. Jpn.* **1984**, *57*, 1556−1561. (b) Yamashita, M.; Tsuruta, E.; Inoue, K.; Oyama, M.; Toriumi, K. *Inorg. Chem.* **1993**, *32*, 363−365. (c) Aragoni, M. C.; Area, M.; Coles, S. L.; Devillanova, F. A.; Hursthouse, M. B.; Isaia, F.; Lippolis, V. *Dalton Trans.* **2012**, *41*, 6611−6613.
(22) For octahedral Ni complexes coligated with I^- ligands, see: (a) Hawkinson, S. W.; Fleischer, E. B. *Inorg. Chem.* **1969**, *8*, 2402−2410. (b) Johnston, D. L.; Horrocks, W. D. *Inorg. Chem.* **1971**, *10*, 687−691. (c) Jones, R. M.; Goldcamp, M. J.; Krause, J. A.; Baldwin, M. J. *Polyhedron* **2006**, *25*, 3145−3158.
(23) Lehmann, U. Ph.D. Dissertation, Universität Leipzig, 2013.
(24) Related Ni_2 complexes with a similar $N_3Ni(\mu\text{-}S_2)NiN_3$ core but a less encumbered binding cavity readily bind a variety of other coligands, see Lozan, V.; Syre, R.; Kersting, B. *Z. Anorg. Allg. Chem.* **2008**, *634*, 2330−2336.
(25) (a) Morassi, R.; Bertini, I.; Sacconi, L. *Coord. Chem. Rev.* **1973**, *11*, 343−402. (b) Mazurek, W.; Philip, A. T. *J. Chem. Soc., Chem. Commun.* **1970**, 184−185.
(26) Lee, K.; Lozan, V.; Langford, S.; Kersting, B. *Dalton Trans.* **2009**, 7481−7485.
(27) (+)-ESI-MS for **5**(ClO_4) in MeCN/MeOH: m/z = 803.3 $[Ni_2(L^{Me2H4})(\mu\text{-}F)]^+$. (+)-ESI-MS for **6**$(ClO_4)$ in MeCN/MeOH: m/z = 821.2 $[Ni_2(L^{Me2H4})(\mu\text{-}Cl)]^+$, see Supporting Information.
(28) For octahedral nickel(II) complexes, ν_1 provides a direct measure for the octahedral splitting parameter Δ_o (Δ_o [cm^{-1}] = $1 \times 10^7/\nu_1$ [nm]); see Lever, A. B. P. *Inorganic Electronic Spectroscopy,* 2nd ed.; Elsevier Science: Amsterdam, 1984.
(29) Smithrud, D. B.; Sanford, E. M.; Chao, I.; Ferguson, S. B.; Carcanague, D. R.; Evanseck, J. D.; Houk, K. N.; Diederich, F. *Pure Appl. Chem.* **1990**, *62*, 2227−2236.
(30) Chaumont, A.; Wipff, G. *New. J. Chem.* **2006**, *30*, 537−545.
(31) Adrian, J. C.; Wilcox, C. S. *J. Am. Chem. Soc.* **1991**, *113*, 678−680.
(32) The (+)-ESI-MS spectrum of **4**$(I)_2$ in MeCN shows two peaks at m/z = 392.2 and 911.2 attributed to the $[Ni_2(L^{Me2H4})]^{2+}$ dication and a monocationic $[Ni_2(L^{Me2H4})]I^+$ contact ion pair, respectively, see Supporting Information.
(33) At the present stage, binding of OH^- or N_3^- cannot be ruled out.
(34) Tamayo, A.; Casabó, J.; Escriche, L.; Lodeiro, C.; Covelo, B.; Brondino, C. D.; Kivekäs, R.; Sillampää, R. *Inorg. Chem.* **2006**, *45*, 1140−1149.
(35) Hossain, M. A.; Llinares, J. M.; Miller, C. A.; Seib, L.; Bowman-James, K. *Chem. Commun.* **2000**, 2269−2270.
(36) Perspective views of complexes **5**(F)·5EtOH·$2H_2O$, **7**(Br)·2MeCN, and **4**(I_2)·3*t*BuOH·MeOH, showing intermolecular hydrogen bonding interactions, are supplied in the Supporting Information (Figures S2, S3, S14).
(37) (a) Gampp, H.; Maeder, M.; Meyer, C. J.; Zuberbühler, A. D. *Talanta* **1985**, *32*, 95−101. (b) Gampp, H.; Maeder, M.; Meyer, C. J.; Zuberbühler, A. D. *Talanta* **1985**, *32*, 257−264. (c) Gampp, H.; Maeder, M.; Meyer, C. J.; Zuberbühler, A. D. *Talanta* **1985**, *32*, 1133−1139.
(38) Convergence difficulties were encountered when processing the vis−NIR data set shown in Figure 4a.
(39) (a) Gans, P.; Sabatini, A.; Vacca, A. *Talanta* **1996**, *43*, 1739−1753. (b) Gans, P.; Sabatini, A.; Vacca, A. *Ann. Chim. (Rome, Italy)* **1999**, *89*, 45−49.
(40) Ahrland, S.; Rosengren, K. *Acta Chem. Scand.* **1956**, *10*, 727−734.
(41) Dietrich, B.; Guilhem, J.; Lehn, J.-M.; Pascard, C.; Sonveaux, E. *Helv. Chim. Acta* **1984**, *67*, 91−104.
(42) Boiocchi, M.; Del Bocca, L.; Gomez, D. E.; Fabbrizzi, L.; Licchelli, M.; Monzani, E. *J. Am. Chem. Soc.* **2004**, *126*, 16507−16514.
(43) Khan, M. A.; Cronier, D.; Bouet, G. M.; Vierling, F. *Transition Met. Chem.* **1995**, *20*, 369−371.
(44) Suzuki, H.; Ishiguro, S. *Bull. Chem. Soc. Jpn.* **1993**, *66*, 83−88.
(45) The same evolution of spectra was observed when $N(n\text{-}Bu)_4Br$ was used instead of NH_4Br, see Supporting Information, Figure S10.
(46) τ is defined as $(\alpha - \beta)/60°$, where α = largest angle, β = second largest angle (τ = 1.0 for an ideal trigonal bipyramid; τ = 0.0 for an ideal square pyramid). Addison, A. W.; Rao, T. N.; Reedijk, J.; Van Rijn, J.; Verschoor, G. C. *J. Chem. Soc., Dalton Trans.* **1984**, 1349−1356.
(47) Gressenbuch, M.; Lozan, V.; Steinfeld, G.; Kersting, B. *Eur. J. Inorg. Chem.* **2005**, 2223−2234.
(48) Reger, D. L.; Foley, E. A.; Watson, R. P.; Pellechia, P. J.; Smith, M. D.; Grandjean, F.; Long, G. J. *Inorg. Chem.* **2009**, *48*, 10658−10669.
(49) Mahoney, J. M.; Beatty, A. M.; Smith, B. D. *J. Am. Chem. Soc.* **2001**, *123*, 5847−5848.
(50) Brammer, L.; Bruton, E. A.; Sherwood, P. *Cryst. Growth Des.* **2001**, *4*, 277−290.

DOI: 10.1021/acs.inorgchem.5b00123
Inorg. Chem. 2015, 54, 3937−3950

(51) Ionic radii of the halide ions are 1.285 Å (F^-), 1.91 Å (Cl^-), 1.96 Å (Br^-), 2.20 Å (I^-), see (a) Shannon, R. D.; Prewitt, C. T. *Acta Crystallogr., Sect. B* **1969**, *25*, 925−946. (b) Shannon, R. D. *Acta Crystallogr., Sect. A* **1976**, *32*, 751−767.
(52) (a) Farnham, W. B.; Roe, D. C.; Dixon, D. A.; Calabrese, J. C.; Marlow, R. L. *J. Am. Chem. Soc.* **1990**, *112*, 7707−7718. (b) Laughrey, Z. R.; Upton, T. G.; Gibb, B. C. *Chem. Commun.* **2006**, 970−972. (c) Zhu, S. S.; Staats, H.; Brandhorst, K.; Grunenberg, J.; Gruppi, F.; Dalcanale, E.; Lützen, A.; Rissanen, K.; Schalley, C. A. *Angew. Chem.* **2008**, *120*, 800−804; *Angew. Chem., Int. Ed.* **2008**, *47*, 788−792. (d) Engeldinger, E.; Armspach, D.; Matt, D.; Jones, P. G. *Chem.—Eur. J.* **2003**, *9*, 3031−3105.
(53) Klingele, M. H.; Steinfeld, G.; Kersting, B. *Z. Naturforsch., B: Chem. Sci.* **2001**, *56*, 901−907.
(54) STOE & Cie GmbH. *X-AREA and X-RED32;* Stoe & Cie GmbH: Darmstadt, Germany, 2012.
(55) Sheldrick, G. M. *Acta Crystallogr., Sect. A* **1990**, *46*, 467−473.
(56) Sheldrick, G. M. *SHELXL-97,* Computer program for crystal structure refinement; University of Göttingen: Göttingen, Germany, 1997.
(57) Spek, A. L. *PLATON - A Multipurpose Crystallographic Tool;* Utrecht University: Utrecht, The Netherlands, 2000.
(58) Farrugia, L. J. *J. Appl. Crystallogr.* **1997**, *30*, 565−568.
(59) Alderighi, L.; Gans, P.; Ienco, A.; Peters, D.; Sabatini, A.; Vacca, A. *Coord. Chem. Rev.* **1999**, *184*, 311−318.
(60) Perdew, J.; Burke, K.; Ernzerhof, M. *Phys. Rev. Lett.* **1996**, *77*, 3865−3868.
(61) Perdew, J.; Burke, K.; Ernzerhof, M. *Phys. Rev. Lett.* **1997**, *78*, 1396−1396.
(62) Adamo, C.; Barone, V. *J. Chem. Phys.* **1999**, *110*, 6158−6170.
(63) (a) Neese, F. *J. Chem. Phys.* **2003**, *119*, 9428−9444. (b) Neese, F. *Int. J. Quantum Chem.* **2001**, *83*, 104−114.
(64) http://www.thch.uni-bonn.de/tc/orca/.
(65) Schaefer, A.; Horn, H.; Ahlrichs, R. *J. Chem. Phys.* **1992**, *97*, 2571−2577.
(66) Klamt, A.; Schüürmann, G. *J. Chem. Soc., Perkin Trans. 2* **1993**, *220*, 799−805.
(67) Van Wüllen, C. *J. Chem. Phys.* **1998**, *109*, 392−399.

DOI: 10.1021/acs.inorgchem.5b00123
Inorg. Chem. 2015, 54, 3937−3950